Orientation and Electronic Structure of the Primary Donor Radical Cation $P_{700}^{+\bullet}$ in Photosystem I: A Single Crystals EPR and ENDOR Study

Hanno Käss,† Petra Fromme, Horst T. Witt, and Wolfgang Lubitz*

Max-Volmer-Institut für Biophysikalische Chemie und Biochemie, Technische Universität Berlin, Str. d. 17. Juni 135, D-10623 Berlin, Germany

Received: September 13, 2000; In Final Form: November 27, 2000

The primary donor in single crystals of photosystem I (PS I) obtained from the thermophilic cyanobacterium *Synechococcus elongatus* is investigated by EPR and ENDOR techniques. The cation radical $P_{700}^{+\bullet}$ was generated chemically or photolytically in the single crystals, and angular dependent spectra were obtained at a temperature of 100 K in the frozen state. The principal values and corresponding axes orientations were determined for three different proton hyperfine coupling (hfc) tensors. On the basis of the tensor magnitudes, their symmetry, and the relative orientations of their axes, they were assigned to the protons of three methyl groups of a single chlorophyll (Chl) *a* molecule. From X-ray crystallography of PS I single crystals, it is known that P_{700} is structurally a chlorophyll dimer (Klukas et al., *J. Biol. Chem.* **1999**, *274*, 7361). The EPR/ENDOR experiments show that the second chlorophyll half carries no or very little ($\leq$15%) spin density. The molecular plane of the spin-carrying Chl *a* molecule in $P_{700}^{+\bullet}$ is parallel to the crystallographic *c* axis. From the orientation of the hf tensors of the methyl groups with respect to this axis, the orientation of the Chl *a* molecule could be determined. The orientation of this Chl *a* is very similar to that of the two symmetrically placed bacteriochlorophyll molecules forming the primary donors P_{865} and P_{960} in the RC of the purple bacteria *Rhodobacter sphaeroides* and *Rhodopseudomonas viridis*, respectively. These results indicate a structural similarity of the electron donors in purple bacteria and photosystem I and point to a common evolutionary origin of both types of reaction centers.

Introduction

Photosystem I (PS I) is a large membrane-intrinsic multisubunit protein complex that occurs in all organisms performing oxygenic photosynthesis.[1−5] More than 100 cofactors (~100 Chl *a*, ~20 carotenoids, 3 [4Fe4S] clusters, and 2 phylloquinones) are bound to the 11 protein subunits of Photosystem I. In cyanobacteria PS I occurs *in vivo* as a trimer with a molecular weight of 1020 kDa. It mediates light-induced charge separation across the membrane, i.e., electron transfer (ET) from plastocyanine or cytochrome c_6 at the lumenal side to ferredoxin at the stromal side of the thylakoid membrane. Photosystem I has been isolated, highly purified, and crystallized from the thermophilic cyanobacterium *Synechococcus* (*S.*) *elongatus*,[4,6] and a structural model at 4 Å resolution has been obtained from X-ray structure analysis.[7−10] The two largest protein subunits, PsaA and PsaB, carry the cofactors of the electron transport chain and most of the antenna chlorophylls and carotenoids. They are related to each other by an approximate local 2-fold symmetry axis (pseudo-C_2 axis). The arrangement of cofactors involved in the ET process is shown schematically in Figure 1 together with the main pigment molecule, chlorophyll (Chl) *a*. These cofactors (from P_{700} to the first FeS center) are also related by the pseudo-C_2 axis.

The light-induced charge separation in PS I starts with singlet excitation of the primary donor, P_{700}, followed by fast electron donation to a chain of electron acceptors comprising two further pairs of chlorophylls, two quinones, and three [4Fe4S] centers.[8,5,10] The involvement of both pigment branches in the ET process has recently been proposed.[11] The single-electron-transfer process leads to the formation of a radical cation of the primary donor and, in subsequent steps, to radical anions of all electron acceptors. Consequently, EPR has played a major role in the identification and characterization of these radicals.[12−14] A detailed picture of the electronic structure is obtained by application of advanced techniques such as electron-nuclear-double resonance (ENDOR)[15−17] and electron spin-echo envelope modulation (ESEEM).[18] These techniques are able to resolve the hyperfine coupling constants with the magnetic nuclei in the radicals that provide direct access to the unpaired electron spin density distribution in the frontier orbitals of the molecule.

The photochemically active species, P_{700}, is of central importance in the primary act of photosynthesis, since it is located at the interface of excitation transfer in the light-harvesting system and electron transfer in the reaction center (RC). This species is distinct from all other chlorophylls by its spectral and redox properties.[5] From the X-ray structure analysis, it is evident that two chlorophyll molecules form the primary donor P_{700}.[8,9] The determination of the orientation and the electronic structure of the primary electron donor is essential for the understanding of the key event in photosynthesis.

It is well established from X-ray crystallography[19] that the primary donor in purple bacterial RCs is a dimer of bacteriochlorophyll (BChl) molecules. The two BChl's are excitonically coupled and provide a trap for the excitation energy from the

* Corresponding author. E-mail: lubitz@echo.chem.tu-berlin.de. Fax: +49 30 314 21122.

† Present address: Institute of Physical and Theoretical Chemistry, Johann Wolfgang Goethe-Universität Frankfurt, Marie-Curie-Str. 9-11, 60439 Frankfurt/M., Germany.

10.1021/jp0032311 CCC: $20.00
Published on Web 01/17/2001

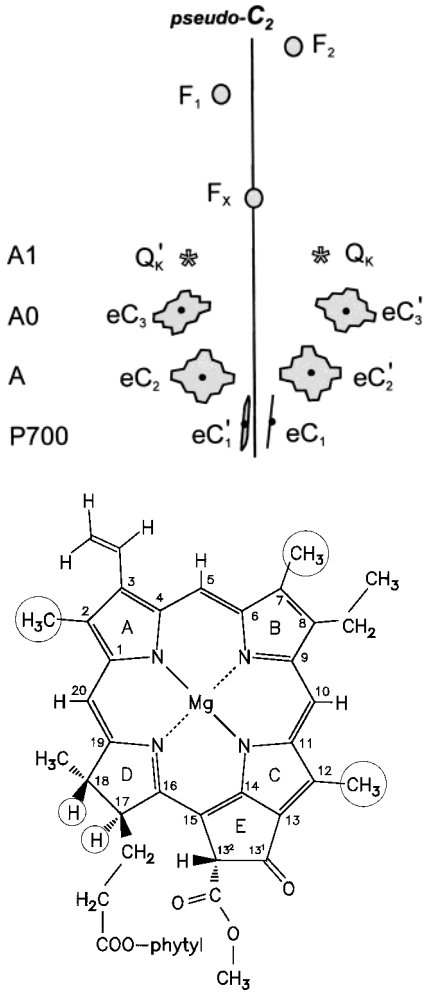

Figure 1. Top: Arrangement of the cofactors constituting the electron transport chain in photosystem I according to ref 9. Shown are six chlorophylls eC_1-eC_3 and $eC_1'-eC_3'$ of the two cofactor branches; two chlorophylls form the primary donor P_{700} (eC_1'/eC_1). The two phylloquinones (vitamin K_1) are labeled with Q_K and Q_K' and the three 4Fe4S centers with F_X, F_1, and F_2. Bottom: Structure of chlorophyll *a* (Chl *a*) with IUPAC numbering of molecular positions. In the $C13^2$ epimer (Chl *a*′), the two substituents at $C13^2$ are exchanged. Bacteriochlorophyll (BChl) *a* has an acetyl group at position 3 instead of vinyl, and the C_7-C_8 double bond is hydrogenated; BChl *b* is similar to BChl *a* but has a vinylidene group at position 8.

antenna system. Furthermore, the oxidation potential of the primary donors is lowered, i.e., adjusted for efficient charge separation in the RC.[20] EPR, ENDOR, and ESEEM techniques showed that these dimers are correctly described as supermolecules with a molecular wave function, carrying the unpaired electron, that is delocalized over both halves of the dimer.[21−25] In general, an asymmetric electron spin density distribution has been found both for BChl *a*- and BChl *b*-containing dimers,[22,26] and implications for the function of these dimeric species have been discussed in the literature.[23,27,28]

In PS I, a pair of chlorophyll molecules, functioning as primary electron donor, was already suggested 30 years ago by Döring et al.[29] This was later supported by EPR work of Norris et al.,[30,31] who postulated that the unpaired electron in $P_{700}^{+\bullet}$ is shared equally by two chlorophyll molecules ("special pair" hypothesis[30]). This was based on the observed reduction of the EPR line width and some limited information on the hfc's from ENDOR experiments.[31,32] The early work in this field was extensively reviewed,[13,21] and different dimer models were proposed in the literature.[33]

In subsequent years, the dimeric nature of $P_{700}^{+\bullet}$ was questioned by several groups, and monomeric chlorophylls were proposed to function instead as the primary donor in PS I. Wasielewski et al.[34] compared the second moment of the EPR line of Chl $a^{+\bullet}$ and $P_{700}^{+\bullet}$, which were deuterated and highly enriched in ^{13}C. Their results indicate a monomeric nature for $P_{700}^{+\bullet}$, i.e., the unpaired electron resides on one Chl *a* molecule. In another paper, Wasielewski et al. proposed that $P_{700}^{+\bullet}$ contains a monomeric chlorophyll *a* enol,[35] which has a significantly lower oxidation potential than Chl *a*, as also observed for P_{700}. On the basis of ^1H ENDOR experiments on $P_{700}^{+\bullet}$ in frozen solutions of PS I, O'Malley and Babcock[36] proposed that the interaction of chlorophyll with its protein environment could cause a mixing of the doublet ground state with a close-lying first excited doublet state in $P_{700}^{+\bullet}$ (see also ref 37). This would lead to a hybrid orbital in the Chl radical in which the electron is delocalized. The ^1H hfc's measured in this work were interpreted by postulating a monomeric Chl $a^{+\bullet}$ for $P_{700}^{+\bullet}$ having a perturbed electronic structure arising from environmental effects. This approach has been recently questioned by Käss et al.[38]

The first ^1H ENDOR and TRIPLE resonance experiments of $P_{700}^{+\bullet}$ in liquid solution at ambient temperature[17,39] showed that the high molecular weight of the PS I particles led to slow tumbling in solution, yielding spectra that resembled those in the frozen state. Isotropic hyperfine coupling constants (hfc's) that are directly related to the spin density at the respective nuclei could therefore not be determined, and a reliable assigment of hfc's to molecular positions could not be given. Attempts to simulate the EPR line of $P_{700}^{+\bullet}$ on the basis of various trial assignments indicated that the system is better described by a monomeric Chl $a^{+\bullet}$ than by a dimer.[39]

The number of different ^1H nuclei coupled to a Chl $a^{+\bullet}$ monomer and in particular to a dimer is very large, which leads to very complex ^1H ENDOR spectra. Consequently, attempts have been undertaken to measure the hf and quadrupole tensors of ^{14}N in Chl $a^{+\bullet}$ and $P_{700}^{+\bullet}$ and also the hfc's of ^{15}N nuclei in respectively labeled material, using ENDOR and ESEEM techniques.[25,40−45] The work of Käss et al.[42,43] indicated that the unpaired electron is delocalized asymmetrically in a Chl *a* dimer, forming $P_{700}^{+\bullet}$. ^{14}N ESEEM experiments on PS I single crystals[44] were interpreted to result from five nitrogen nuclei; the fifth was tentatively assigned to the second half of a Chl dimer forming $P_{700}^{+\bullet}$. In the recent work of Babcock and co-workers,[45] who used a combination of isotope labeling ($^{14}N/^{15}N$), multifrequency ESEEM, ENDOR, and spectral simulations, only four sets of nitrogen couplings have been determined and assigned to one monomeric Chl $a^{+\bullet}$. Further work by the same group showed, however, that one nitrogen from a histidine can also be detected that is ligated to this chlorophyll.[41] This is in agreement with the work of Webber,[46] Redding,[47] and Krabben[48] and co-workers, who identified one histidine in protein subunit PsaB as a putative ligand of the spin-carrying chlorophyll in $P_{700}^{+\bullet}$.

The character of P_{700} has also been probed by vibrational spectroscopy.[49−52] In a recent FTIR study of $P_{700}/P_{700}^{+\bullet}$, Breton et al.[51] claimed that $P_{700}^{+\bullet}$ is a fairly strongly delocalized dimeric species, which is in contrast to the recent findings from EPR techniques. An interesting finding, however, is the observation of a broad mid-infrared band at 3300 cm^{-1} that

indicates the presence of a chlorophyll dimer forming the primary donor.[51]

The detailed electronic structure of $P_{700}^{+\bullet}$ and the arrangement of the chlorophylls are important for establishing structural and functional similarities and differences between the primary donors of PS I and the related species in PS II and purple bacterial RCs and for a better understanding of the function of these species that act at very different redox potentials. In principle, both types of information can be obtained from a determination of the individual hfc tensor magnitudes and axes orientations of the various magnetic nuclei in $P_{700}^{+\bullet}$. The full hyperfine tensors can be measured by ENDOR experiments performed on PS I single crystals. In this paper, we report on the first ENDOR investigation on $P_{700}^{+\bullet}$ in PS I single crystals from *Synechococcus elongatus*.

Materials and Methods

Preparation and Crystallization of PS I from *Synechococcus elongatus*. PS I was isolated and purified from the thermophilic cyanobacterium *Synechococcus elongatus* as described in ref 6. The crystallization of PS I was performed by dialysis against low salt concentration similar to the procedure described by Fromme and Witt.[6] To get large crystals useful for X-band ENDOR experiments, we modified the conditions for crystallization. The protein concentration was increased to 90 mg/mL, which is the solubility limit for PS I at a salt concentration of 50 mM $MgSO_4$ at 4 °C. A small microdialysis chamber (diameter 3 mm) was used and filled to a height of 2 mm. The salt concentration was then decreased in two steps. During 1 day, it was reduced to 30 mM; subsequently, a linear gradient from 30 mM to 12 mM $MgSO_4$ was established in order to get an optimum yield of germination versus crystal growth. The crystals grew within 3−4 days in shapes of hexagonal needles or hexagonal plates. The crystals were stored in a solution containing 5 mM MES, pH 6.4, and 0.02% β-dodecyl maltoside (β-DM) for a maximum of 2 days at 4 °C prior to the EPR and ENDOR experiments.

Characterization of Single Crystals. The PS I single crystals used for the measurements were either needle-shaped or had the form of hexagonal plates. The needles were 2−3 mm long and had a diameter of 0.5 mm. The hexagonal plates had a diameter of about 1.5 mm and a height of 0.5 mm. The concentration of PS I (and P_{700}) in the single crystals was estimated to be 1 ± 0.1 mM. This equals a Chl concentration of 100 mM Chl, with a Chl/P_{700} ratio of about 100.

The crystallographic space group is $P6_3$. The crystal unit cell is hexagonal with cell constants $a = b = 286$ Å and $c = 167$ Å.[53] In the frozen state, the unit cell constants are decreased to $a = b = 281$ Å and $c = 165$ Å.[54] In the needle-shaped crystals, the crystallographic *c* axis is oriented parallel to the needle axis; in the hexagonal plates, it is parallel to the plane normal. The symmetry elements are given in Figure 2. The unit cell contains two PS I trimers, with one monomer in the asymmetric unit. Six PS I monomers are found on inequivalent sites of the unit cell.

Crystal Mounting. The crystal holders were constructed in our laboratory from PCTFE (Kel-F) purchased from Huth & Söhne (Starnberg, Germany). The holders consist of two parts, one of them carrying the crystal, the other one serving as a protective cap (see Figure 3). The o.d. of 4 mm is small enough to insert the holder into our ENDOR cavity/Dewar system. Before mounting, the crystals were soaked for 10 min in a 1.5 M solution of sucrose in MES buffer at room temperature. They were then placed on the flat vertical plane of the holder, together with a drop of mother liquor. Depending on the desired orientation of the unit cell, needle-shaped or plate-like crystals were used. Needle-shaped crystals were oriented with their *c* axis parallel to the rotation axis of the holder (Figure 3, right). Mounting of plates automatically orients the *c* axis perpendicular to the rotation axis (Figure 3, left). Excess mother liquor was removed with a paper tip, and the holder was immersed quickly into liquid nitrogen. The remaining solution fixed the crystal irreversibly after freezing on the holder. Then the crystal holder was sealed with the cap that was filled with liquid nitrogen. This prevents thawing when transferring the holder to the spectrometer. The misalignment of the crystal *c* axis relative to the desired orientation was $\leq \pm 5°$. For plate-like crystals, the orientational error was smaller ($\leq \pm 2°$).

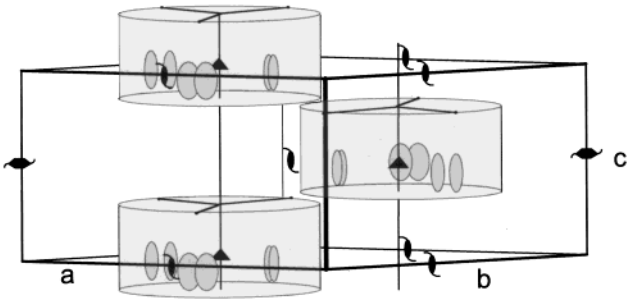

Figure 2. Schematic representation of the unit cell of the PS I single crystal with the appropriate symmetry elements.[53] The crystallographic axes are labeled *a*, *b*, and *c*. Each unit cell contains two PS I trimers. These are schematically symbolized by shaded cylinders. The chlorophylls constituting the primary donors are enlarged and indicated by shaded ovals. The view is roughly along the line bisecting the *a*,*b* plane. Note that the plane of the chlorophyll molecules is approximately parallel to the 6-fold axis (*c* axis). This axis is parallel to the pseudo-C_2 axis of the PS I electron transport chain (see Figure 1).

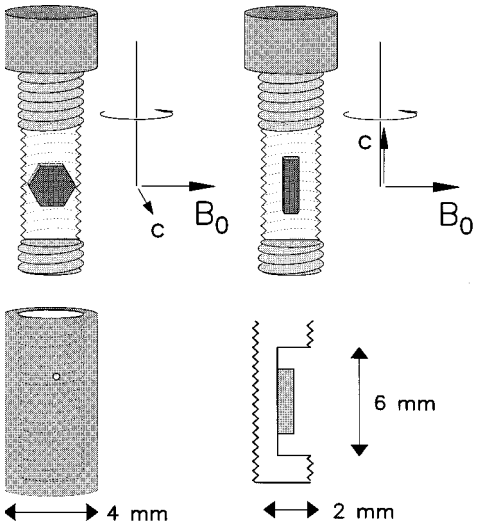

Figure 3. Top: Holder for EPR/ENDOR experiments on single crystals, made from Kel-F. The positioning is shown for hexagonal plates (left) and for needle-shaped crystals (right). Bottom: A side view of the holder with the mounted crystal (right), and the screw cap for the holder (left) is shown. The holder could be rotated inside the cavity around its long axis which is oriented perpendicular to the static magnetic field, B_0 (see axes system).

Solution Samples. The PS I samples used in the liquid and frozen solution ENDOR experiments were prepared in a buffer containing 20 mM MES-Na, 200 mM $MgSO_4$, and 0.02% β-DM at a pH value of 6.4. The particles in this solution were trimeric complexes of PSI; the molecular weight of a trimeric PS I protein is about 1020 kDa. The samples had a Chl concentration

of 9.8 mg/mL, corresponding to a concentration of about 100 μM in P_{700}. For ENDOR samples in liquid solution, Pyrex glass capillaries of 1 mm i.d. were used to minimize dielectric losses in the cavity. For frozen solution samples, quartz capillaries of 4 mm o.d. and 3 mm i.d. (Wilmad SQ 727) were employed.

Oxidation of P_{700}. Light oxidation was done by illuminating the mounted crystals at room temperature for 1 min with a 150 W tungsten projection lamp equipped with a heat protection filter before freezing in the light. Alternatively, the primary donor was also oxidized chemically in the single crystals with $K_3[Fe(CN)_6]$. The crystals tolerate an incubation of 16 h at room temperature in the dark in a buffer solution containing 3 mM $K_3[Fe(CN)_6]$. Before freezing, the crystals were incubated for 10 min in a solution containing 1 mM $K_3[Fe(CN)_6]$, 5 mM MES-Na, pH 6.4, 0.02% β-DM, and 1.5 M sucrose. To further increase the signal intensity of $P_{700}^{+\bullet}$ in the chemically oxidized crystals, we illuminated some of the crystals additionally for 10 min at 77K in a transparent dewar filled with liquid nitrogen.

For ENDOR experiments in liquid solution, the cation radical $P_{700}^{+\bullet}$ was generated by continuous illumination of the sample inside the EPR/ENDOR cavity with a 100 W tungsten halogen lamp equipped with a water filter of 8 cm path length and a Schott RG 660 short wavelength cutoff filter. The samples for frozen solution experiments were illuminated at room temperature for 1 min with a 1000 W tungsten projection lamp using a water filter of 10 cm path length. Subsequently, the samples were quickly frozen under illumination in liquid nitrogen to stabilize the charge separated state and then transferred to the spectrometer. Investigation of these optically oxidized $P_{700}^{+\bullet}$ samples gave results identical to those that were oxidized with 10−20 mM $K_3[Fe(CN)_6]$.

EPR/ENDOR Spectroscopy. The EPR and ENDOR measurements were performed on a Bruker ESP 300 E spectrometer with laboratory-built ENDOR and special TRIPLE[16,22] accessories. The liquid solution experiments were carried out using a TM_{110} cavity of local design,[55,56] providing a high Q factor ($\sim$ 5000). In this cavity, the sample temperature was controlled by a Bruker ER 4111 VT nitrogen gas flow system operating in the range of 110−300K. The frozen solution and single-crystal spectra were taken in a cavity of similar design[56] fitted to an Oxford 910 A helium-flow cryostat (temperature range, 1.9−250K).

Analysis of ENDOR Spectra. The presence of overlapping lines in the single crystal ^{1}H ENDOR spectra of $P_{700}^{+\bullet}$ made it necessary to employ a spectral deconvolution program[22,57] for the determination of the individual line positions. This program is used to simulate the spectra by superposition of an appropriate number of single Lorentzian lines. Line positions, widths, and amplitudes are optimized by means of a Simplex algorithm.

The ENDOR resonance condition for the hyperfine transition frequency $\nu_\pm$ of a nucleus with $I = {}^1/_2$ coupled to an electron spin ($S = {}^1/_2$) by an isotropic hyperfine coupling (hfc) A_{iso} is[16]

$$\nu_\pm = |\nu_n \pm A_{iso}/2| \tag{1}$$

At a magnetic field of 0.3450 T, the Larmor frequency of ^{1}H is $\nu_n = \nu^1_H = 14.69$ MHz. For most organic π radicals, the magnitude of the proton hfc A_{iso} is less than $2\nu^1_H$, and the ENDOR lines are displaced symmetrically around ν^1_H.

The occurrence of only isotropic hfc's in a spectrum is a special case for small molecules rapidly tumbling in liquid solution, by which all anisotropic hfc components are averaged out. This is not the case for the trimeric PS I complex with its very large molecular weight (>1 MDa). In general, the hfc's depend on the relative orientation of the electron spin and the nuclear spin with respect to the external magnetic field, $\vec{B}_0$, and they are described by a hfc tensor **A**. In case of an isotropic electronic g factor, the resonance condition is[58]

$$\nu_\pm = \sqrt{\nu_n^2 + \frac{1}{4}(\vec{r}\cdot\mathbf{A})\cdot(\mathbf{A}\cdot\vec{r}) \mp \nu_n\cdot\vec{r}\cdot\mathbf{A}\cdot\vec{r}} \tag{2}$$

with $r = \vec{B}_0/|B_0|$. This directly yields the transition frequencies under a rotation of the magnetic field, $\vec{B}_0$, in the ij symmetry plane. For an angle, φ, between $\vec{B}_0$ and the i axis, we obtain

$$\frac{1}{2\nu_{^1H}}(\nu_-^2 - \nu_+^2) = A_{ii}\cos\varphi + A_{jj}\sin\varphi + 2A_{ij}\sin\varphi\cos\varphi \tag{3}$$

which in the limit of small nondiagonal elements ($|A_{ij}| \ll \nu^1_H$) results in[22]

$$\nu_\pm = \nu_n \pm |\frac{1}{4}(A_{ii} + A_{jj}) + \frac{1}{2}\sqrt{\frac{(A_{ii} - A_{ij})^2}{4} + A_{ij}^2}\cos 2(\varphi - \varphi_o)| \tag{4a}$$

$$= \nu_n \pm |\frac{1}{2}A_{ii}\cos^2\varphi + \frac{1}{2}A_{jj}\sin^2\varphi + \frac{1}{2}A_{ij}\sin 2\varphi| \tag{4b}$$

$$= \nu_n \pm |\frac{1}{4}(A_{ii} + A_{jj}) + \frac{1}{4}(A_{ii} - A_{jj})\cos 2\varphi + \frac{1}{2}A_{ij}\sin 2\varphi| \tag{4c}$$

$$\text{with } \tan 2\varphi_o = 2A_{ij}/(A_{ii} - A_{jj})$$

For the evaluation of the hfc tensor elements, eq 4c was fitted to the ENDOR line positions determined from the experimental data with the deconvolution program described above.

Results

EPR Experiments on $P_{700}^{+\bullet}$ in Solution and Single Crystals. X-band EPR of $P_{700}^{+\bullet}$ in PS I of *Synechococcus elongatus* in liquid solution yielded an unresolved inhomogeneously broadened line exhibiting a line width ΔB_{pp} of 0.700 mT (±0.005) and a g factor of 2.0025 (±0.0001). In frozen solution, the line width increased slightly to 0.715 mT at 165 K and reached 0.785 mT at 10 K. This result is consistent with former investigations.[59,31,60] In single crystals at 100 K, ΔB_{pp} was 0.75(1) mT. Within experimental error, no angle-dependent variations of the EPR line width and the effective g factor could be detected at X-band frequencies. The g tensor of $P_{700}^{+\bullet}$ was determined at 140 GHz,[61] with higher precision at frequencies above 300 GHz,[62] and very recently also in single crystals of *S. elongatus* at 94 GHz.[63] The resulting small total anisotropy ($g_{max} - g_{min}$) $\approx 9 \times 10^{-4}$ is less than that found for the primary donor radical cation $P_{865}^{+\bullet}$ determined in RC single crystals of *Rb. sphaeroides* ($\sim 13 \times 10^{-4}$).[64] Thus, the approximation of an isotropic g factor made in eq 2 (see below) will cause no significant errors in our data analysis.

ENDOR Experiments on $P_{700}^{+\bullet}$ in Liquid and Frozen Solution. Liquid and frozen solution ENDOR spectra of light-induced $P_{700}^{+\bullet}$ at different temperatures are shown in Figure 4. Figure 4a depicts the Special TRIPLE spectrum (283 K) that exhibits larger intensities and better resolution than those of the related ENDOR spectrum (Figure 4b). The spectrum is similar to that observed earlier for $P_{700}^{+\bullet}$ in PS I from other organisms.[39,36,65] The spectra of chemically oxidized $P_{700}^{+\bullet}$ are indistinguishable from those of photolytically oxidized $P_{700}^{+\bullet}$ (data not shown). No differences in the ENDOR spectra are found for PS I samples prepared with different detergents (e.g., Triton X-100 and β-DM) and different detergent concentrations.

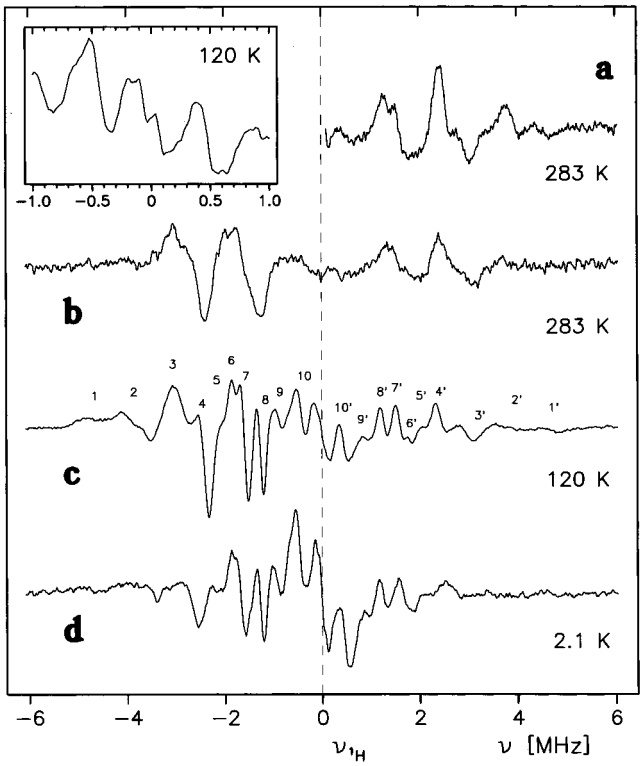

Figure 4. ENDOR on $P_{700}^{+\bullet}$ in liquid and frozen solutions in PS I of *Synechococcus elongatus*. Characteristic line pairs are labeled in the spectrum at $T = 120$ K. (a) Special TRIPLE spectrum at 283K. (b−d) ENDOR spectra at 283, 120, and 2.1 K, respectively. Experimental parameters: TM_{110} ENDOR cavity; microwave power 49, 10, 6.3, and 0.79 mW for spectra a, b, c, and d, respectively; radio frequency (RF) power 150 W, in liquid solution 450 W (B_2 field for 500 W RF power was 2.5 mT at 14 MHz); effect modulation frequency 12.5 kHz at 283 K and 3.13 kHz at 120 and 2.1K; time constant (TC) 1.25 s and accumulation time (TM) 21 × 320 s for special TRIPLE; TC 1.25 s, TM 16 × 400 s for ENDOR at 283 K; TC 640 ms, TM 8 × 400 s at 120 and 2.1 K; frequency modulation (FM) 111 kHz for special TRIPLE, 200 kHz for ENDOR at 283 K and 100 kHz for ENDOR at 120 and 2.1 K. Inset: ENDOR region of small hfc's at high resolution for $T = 120$ K, RF power 150 W, FM 20 kHz, and TC 640 ms.

This shows that the electronic structure of $P_{700}^{+\bullet}$ is not influenced by the detergent, in contrast to the effects detected for P^+ in bacterial RCs,[66] leading to the assumption that P_{700} in PS I is better shielded from the surrounding solution than the primary donor in purple bacterial RCs. The hf splittings observed at 120 K (Figure 4c) are given in Table 1, together with an assignment derived from the experiments on the single crystals described below.

Comparison between the data obtained in frozen and liquid solution (Figure 4) clearly demonstrates that also in the liquid state, a powder-type ENDOR spectrum is obtained. This is due to the fact that the large trimeric PS I complex is tumbling too slowly in solution at 283 K to effectively average out the hf anisotropies of the various proton nuclei.[67] An estimation yields a rotational correlation time τ_R of $\sim 7 \times 10^{-7}$ s.[68] This shows that only hf anisotropies of ≤ 0.2 MHz can be effectively averaged out. Consequently, all larger hfc's (>2 MHz), even those of CH_3 groups, yield powder-type ENDOR patterns in such spectra (compare panels a and c of Figure 4). ENDOR spectra in liquid solution obtained with constant rf field show a larger intensity of the high-frequency lines due to the hyperfine enhancement factor.[16] This is not the case in the $P_{700}^{+\bullet}$ ENDOR spectra, where the low frequency lines are more intense. This is most likely due to cross-relaxation processes.[16]

TABLE 1: Hyperfine Splittings Obtained from the ENDOR Spectrum in Frozen Solution of $P_{700}^{+\bullet}$ in *Synechococcus elongatus* at 120 K

line pair[a]	hfc[b] [MHz]	assignment[c] position (hf component)
1,1′	9.6	17,18 ($A_{\|\|}$,$A_\perp$)
2,2′	7.7	17,18 ($A_{\|\|}$,$A_\perp$)
3,3′	6.1	12 ($A_{\|\|}$)
4,4′	4.9	12 ($A_\perp$)
5,5′	4.2	7 ($A_{\|\|}$)
6,6′	3.7	2 ($A_{\|\|}$)
7,7′	3.2	7 ($A_\perp$)
8,8′	2.5	2 ($A_\perp$)
9,9′	1.8	n.a.
10,10′	0.9	n.a.

[a] For labeling of line positions, see Figure 4c. [b] Experimental error: ±100 kHz, except for 1,1′ and 2,2′ (±200 kHz). [c] Assignments of hfc's based on experiments on single crystals and evaluation in this work (see Tables 2 and 3); for numbering of molecular positions, see Figure 1. Line pairs 1 and 2 belong to the β-protons of ring D, line pairs 3 to 8 belong to methyl protons, and line pairs 9 and 10 cannot be clearly assigned (n.a.) (see text).

Lowering of the temperature enhances the signal-to-noise (S/N) ratio of the ENDOR spectra. The optimum temperature lies in the range of 100−130 K. The spectrum depicted in Figure 4c at 120 K also shows optimal resolution, with several sharp line pairs from which the hfc's can be obtained (Table 1). From the spectra in solution, no unambiguous assignment of hfc's to molecular positions can directly be achieved. Variations in line intensities between the spectra are due to differences in the temperature dependencies of the relaxation rates of the individual nuclei. This does not affect the evaluated hfc's which change by less than 0.1 MHz in the range from room temperature down to 100 K.

A remarkable change occurs in the $P_{700}^{+\bullet}$ ENDOR spectrum when the temperature is further decreased. Between 60 and 70 K, line pairs 4 and 3 start to change their shape and position. The same effect, although less pronounced, is observed for line pair 7 at lower temperature. The line pairs 1 and 2 also become very broad. The observed effect is fully reversible, and the onset always occurs in the same narrow temperature range. Similar effects have been detected in low-temperature ENDOR experiments with deuterated chlorophyll-type cation radicals[70] and have been attributed to a freezing out of the free rotation of the methyl groups in these species, which complicates the ENDOR spectra. Because of this effect, all spectra of $P_{700}^{+\bullet}$ in the single crystals (see below) have been obtained at 110 K.

ENDOR Experiments of $P_{700}^{+\bullet}$ in PS I Single Crystals. ENDOR measurements were performed on $P_{700}^{+\bullet}$ in the single crystals at the optimum temperature of 110 K. The PS I crystals were rotated in two different planes. The first set of experiments was done for rotation of the crystal around the crystallographic *c* axis in steps of 5° and the second set under rotation around an axis perpendicular to the *c* axis in steps of 10°. The larger number of data points for rotation around the *c* axis was chosen because of the expected 6-fold rotational symmetry, whereas for rotation perpendicular to the *c* axis a 2-fold symmetry is obtained. The experiments were repeated several times both with photoinduced and chemically oxidized $P_{700}^{+\bullet}$ in single crystals. The evaluated hfc's were identical in all cases within experimental error. Because of the relatively poor signal intensity, no ENDOR experiments could be performed at ambient temperatures. Figure 5 shows selected spectra for rotation in both crystallographic planes, together with the powder ENDOR spectrum obtained from $P_{700}^{+\bullet}$ in PS I frozen solutions (top).

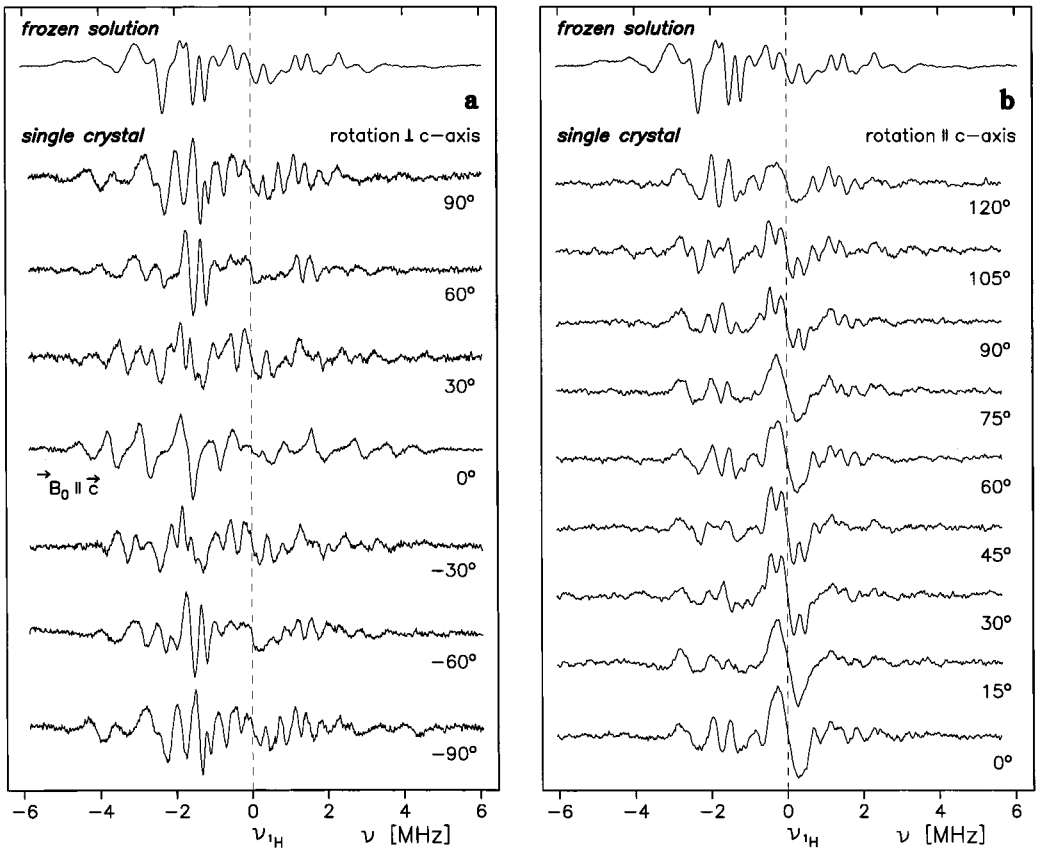

Figure 5. ENDOR on $P_{700}^{+\bullet}$ in single crystals of PS I. Selected spectra for rotation of the crystal (a) perpendicular to and (b) around the crystallographic *c* axis (see Figure 2). The slight deviation of spectra at 0°, 60°, and 120° are due to a misalignment of the *c* axis of the crystal to the rotation axis by ~5°. The spectrum of $P_{700}^{+\bullet}$ in frozen solution of PS I at 120 K (from Figure 4c) is included for comparison (top). Parameters: TM_{110} ENDOR cavity; microwave power 12.6 mW; temperature 100 K; RF power 150 W; effect modulation frequency 12.5 kHz; TC 320 ms; TM 7 × 335 s; FM 140 kHz.

Angular-dependent ENDOR spectra for rotation of the single crystal perpendicular to the *c* axis are depicted in Figure 5a. They exhibit a number of well resolved lines with a minimum linedwidth of about 200 kHz, which increases up to 400 kHz in the outer parts of the spectra. As in the case of PS I in frozen solution, the lines on the low-frequency side are more intense than those on the high-frequency side. Without further deconvolution, a maximum of at least nine resolved line pairs is visible (see orientation ±90°). At 0°, some of the lines coincide, and the S/N ratio increases significantly (note that the spectra are normalized). In this orientation, obviously all six sites are equivalent. This means that the external magnetic field, $\vec{B}_0$, is approximately parallel to the crystallographic *c* axis for this orientation. The expected rotational symmetry of 180° is clearly visible in the spectra (compare orientation −90° and +90°).

ENDOR spectra taken under rotation of the single crystal around the *c* axis are shown in Figure 5b. They exhibit a rotational symmetry of 60°. This is consistent with the X-ray structure analysis, which showed that the crystallographic *c* axis of PS I single crystals is a 6-fold rotational symmetry axis (see Figure 2). Here, the angular dependent line shifts are not as large as those in the case of the rotation perpendicular to the *c* axis. For the analysis of the spectra, a careful deconvolution is necessary because a large number of line pairs is expected due to the six inequivalent sites in the unit cell.

Simulation of the Angular Dependence of hfc's. On the basis of eq 2, a program for the calculation of angular-dependent hfc's was written. It employs the symmetry information (axes of rotational symmetry) resulting from the X-ray structure analysis.[53] Starting with one hfc tensor with arbitrary principal values and orientation relative to the crystal axes, it first determines the orientation of the five other magnetically inequivalent tensors in the unit cell. To determine accidental misalignments, we then rotate the whole tensor set relative to the *a* and *c* axis, as outlined below (Figure 6). Then, ENDOR transition frequencies and hfc's are calculated for a rotation of the unit cell relative to the external magnetic field, $\vec{B}_0$. In the following, a simple convention is used for labeling of planes defined by coordinate axes. For example, the plane containing the A_1 and A_3 principal axes of the hfc tensor is called the "(A_1,A_3) plane".

Rotation Perpendicular to the Crystal c Axis. In the following, a typical set of simulations is described in detail. The geometrical definitions are found in Figure 6 (left). The magnetic field, $\vec{B}_0$, is parallel to the *Z* axis of the laboratory system. The (*X*,*Z*) plane of the laboratory system is assumed to be parallel to the (*a*,*c*) plane of the crystal unit cell. Simulations of the expected angular dependent hfc's for this geometrical arrangement are shown in the right part of Figure 6. For clarity, the figure shows the rotation pattern for only one hfc tensor. The simulation is represented by the solid lines, and the hfc's determined from the experimental ENDOR spectra are given by dots.

In the first simulation (Figure 6, right, top), the angles between the A_{33} axis of the hfc tensor of site 1 and the crystallographic axes *c* and *a* are $\gamma = 33°$ and $\delta = 0°$, respectively. The (A_1,A_3) plane of the tensor system is assumed to be parallel to the (*a*,*c*) plane of the unit cell; therefore, the A_2 principal axis is perpendicular to this plane. The same holds for site 1′. Due to the crystal symmetry, the angle δ is 60° for sites 2,2′ and 3,3′.

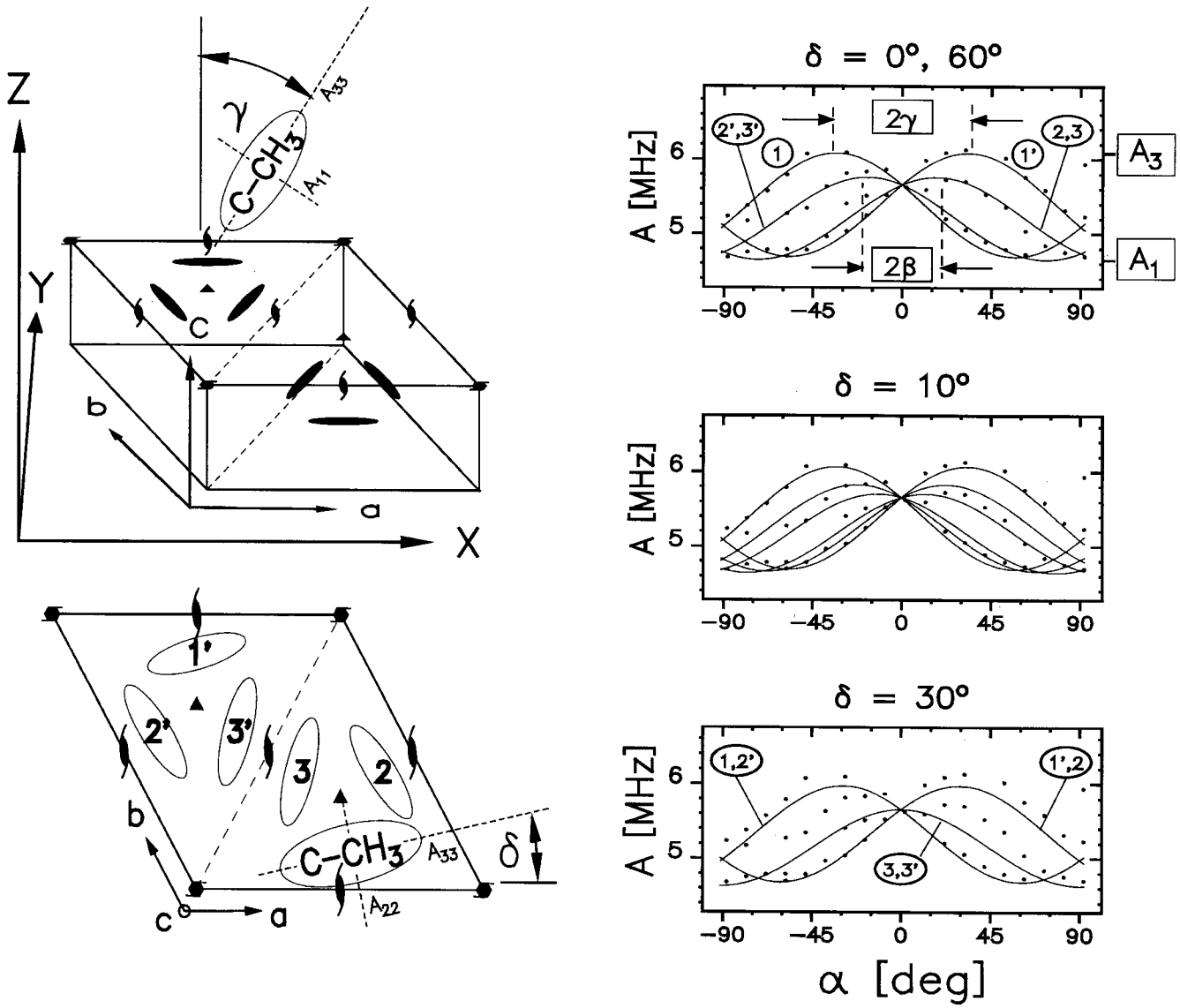

Figure 6. Left, top: Unit cell with two PS I trimers; the P_{700} molecules are indicated as ovals. *X*, *Y*, and *Z* are laboratory coordinates, with $\vec{B}_0$ parallel to the *Z* axis. The simulations (right) shown here were calculated assuming that the (*a*,*c*) plane of the unit cell is always parallel to the (*X*,*Z*) plane; i.e., $\vec{B}_0$ is rotated in the crystallographic (*a*,*c*) plane. The orientation of one methyl hfc tensor in the crystal unit cell is given by angles γ and δ (left). For clarity, only one out of the six hfc tensors on the magnetically inequivalent sites is depicted, including its A_{ii} axes. The orientations of the other five tensors follow from symmetry (see Figure 2). Left, bottom: The numbering of the sites (P_{700}) with 1,2,3 and 1′,2′,3′ corresponds to the labels used in the simulated rotation patterns. Right: Simulation of rotation patterns for one single proton hfc tensor (methyl group) of axial symmetry with principal values of $A_\perp = A_1 = A_2 = 4.70$ MHz and $A_\parallel = A_3 = 6.10$ MHz; rotation perpendicular to the crystallographic *c* axis, $\gamma = 33°$. Instead of the experimental ENDOR line position, the corresponding hyperfine coupling *A* is given directly. Three different δ values were used. Because of the 6-fold rotation symmetry, $\delta = 0°$ is equivalent to $\delta = 60°$. Experimentally determined hfc's are presented by dots (see Table 2). Note that the agreement is obtained for $\delta = 0°$, 60° but not for $\delta = 10°$ or 30°.

The rotation pattern contains four curves, since two pairs are magnetically equivalent, i.e., 2,3 and 2′,3′, whereas 1 and 1′ are single sites. This is reflected in the relative spectral intensities of the actual ENDOR spectrum. The assignment of the curves to specific sites of the unit cell follows the labeling given in the left part of Figure 6. The angle difference between the maxima of curves 1 and 1′ equals 2γ, and that of curves 2,3 and 2′,3′ is 2β. A simple trigonometric calculation shows that $\tan\gamma = 2\tan\beta$. The orientations $\delta = 0°$ and $\delta = 60°$ yield identical rotation patterns because of the 6-fold rotational symmetry.

Further simulations are shown for a rotation of the (A_1, A_3) plane of the initial tensor system by a different angle, δ. For $0° < \delta < 30°$, a pattern consisting of six curves is obtained (Figure 6, right, center) because for these angles, all six sites of the unit cell are magnetically inequivalent. However, for $\delta = 30°$, only three curves are obtained, since the six sites are then arranged in three groups of pairwise magnetically equivalent sites, 1,2′, 1′,2, and 3,3′ (Figure 6, right, bottom). In the same way, simulations were obtained for a rotation of the (A_1,A_3) plane by an angle ϵ around the *a* axis (not shown). Only $\epsilon = 0°$ yields a four-line pattern, whereas for $0° < \epsilon < 90°$, the pattern consists of six curves (in the case of $\epsilon = 90°$, a rotation of the crystal around the crystallographic *c* axis occurs).

As is evident from a comparison of the simulations with the experimental data (panels in Figure 6, right), the calculated line pattern consisting of four curves ($\delta = 0°$; $\epsilon = 0°$) represents the best fit. Thus, it is concluded that in the experiment the static magnetic field, $\vec{B}_0$, was rotated in the (A_1,A_3) plane of the hfc tensor (or in a symmetry-related plane). Considering the ENDOR line width of about 200 kHz found in the experiment, examination of the calculated rotation patterns yields an estimate

of ±5° for the accuracy of the angles evaluated from the measured ENDOR spectra.

In the first set of experiments, the crystal was rotated perpendicular to its *c* axis. The simulations show that $\vec{B}_0$ was rotated in the (A_1,A_3) plane. Thus, both principal values A_1 and A_3 can be determined from this experiment, together with the angle γ between the A_3 principal axis and the crystallographic *c* axis (Figure 6). One single orientation should exist where all six tensors yield the same hfc values, since $\vec{B}_0$ is then parallel to the *c* axis. This is experimentally found for the rotation angle 0° in Figure 5a. It is evident that the phase angle γ between the point where all lines coincide and the maximum hfc splitting in the rotation pattern yields the orientation of the A_3 axis relative to the crystallographic *c* axis (see Figure 6, right, top). In principle, there are three more symmetry-related orientations yielding the same rotation pattern, two of which can be excluded as shown below.

Rotation around the Crystallographic c Axis. The third principal value A_2 of the hfc tensor can be determined from the set of ENDOR spectra obtained for rotation of the crystal around the *c* axis. This is possible, since in the PS I crystals from *S. elongatus* the crystallographic *c* axis lies in the (A_1,A_3) plane of the three evaluated hfc tensors. In addition to A_2, this rotation yields another value, A^*, which depends on the magnitude of A_3 and A_1. It is the maximum hfc that can occur for an orientation of the static magnetic field, $\vec{B}_0$, in the (*a*,*b*) plane of the unit cell. Provided that the principal values of A_1, A_3, and the angle γ between the A_3 principal axis and $\vec{B}_0$ are known, A^* can be easily calculated. Equation 4b gives the general angular dependence of A^*, with $A^* = 2|\nu_\pm - \nu_n|$. The geometrical representation of this equation is an ellipse with principal axes of length $\sqrt{A_i}$ and $\sqrt{A_j}$. After transformation to the principal axis system, A^* becomes

$$A^* = A_1 \cos^2 \gamma + A_3 \sin^2 \gamma \qquad (5)$$

Evaluation and Assignment of the Methyl Proton hfc Tensors. *Evaluation of Complete Rotation Patterns.* The experimentally determined rotation pattern could be separated into the contributions of three different hfc tensors **A**, **B**, and **C** (Figure 7) by comparison of the experimental data with simulations. Subsequently, both sets of ENDOR spectra for rotation of the PS I single crystal around and perpendicular to the crystallographic *c* axis were evaluated by fitting a cosine function (equation 4b) to the data points (see Figure 8). Thereby, a least-squares fitting routine was employed. Since the rotation patterns **A**, **B**, and **C** for a rotation of the crystal perpendicular to the crystallographic *c* axis consist of four lines each, it can be concluded that the (A_1,A_3) planes of all three hfc tensors are parallel within experimental error. Thus, the relative orientations of the methyl hf tensors (e.g. of component A_3) can directly be evaluated (see Figure 6) and compared with the orientations of the C−CH_3 bonds in the chlorophyll molecule. The hfc tensor principal values A_1, A_2, and A_3 of the protons of methyl groups **A**, **B**, and **C** are given in Table 2, together with the angles γ between their respective principal A_3 axes and the crystallographic *c* axis.

The A^* values determined from rotation around the crystallographic *c* axis were 5.4, 4.0, and 2.8 MHz for the three rotation patterns for methyl hfc's labeled **A**, **B**, and **C**, respectively. Within experimental error, they correspond quite well to the values of 5.1, 3.8, and 2.8 MHz calculated from the values A_1, A_3, and γ (Table 2), using eq 5. This shows the consistency of the evaluated results.

The hfc tensors **A** and **C** are axially symmetric to a good approximation; for tensor **B**, the deviation from axial symmetry is somewhat larger (Table 2). From the line intensities and tensor symmetries all three tensors can be assigned to protons of freely rotating methyl groups.[71] In Figure 7 (top), the low-frequency half of the ENDOR spectrum of $P_{700}^{+\bullet}$ in frozen solution is shown. The powder ENDOR lines corresponding to the rotation patterns **A**, **B**, and **C** show the characteristic shape of axially symmetric hfc tensors. An evaluation following ref 72 yields principal values $A_{||}$ and $A_\perp$ (Table 1) which are good estimates for A_3 and the averaged value $(A_1 + A_2)/2$ of the three methyl proton tensors obtained from the single-crystal experiments. A powder ENDOR simulation using the principal values of the three tensors in Table 2 is also shown in Figure 7 (top). The simulation is in very good agreement with the respective lines in the frozen solution ENDOR spectrum of $P_{700}^{+\bullet}$. Note that the $A_{||}$ component of the methyl group at position 12 overlaps with the broad resonances of the β-protons of ring D (positions 17 and 18).

Assignment of the Three hfc Tensors and Orientation with Respect to the c Axis. It can be safely assumed that $P_{700}^{+\bullet}$ is a chlorophyll-type cation radical, since there are no other porphyrinoid pigment molecules present in PS I.[73] The questions that remain to be answered are to which molecular positions the tensors **A**, **B**, and **C** have to be assigned and whether they all belong to one single chlorophyll molecule or not. Answers can be obtained by evaluation of the hfc tensors derived from ENDOR on the PS I single crystals.

On the basis of previous experiments on Chl cation radicals, the most prominent lines are expected for freely rotating methyl groups. Only three methyl substituents are directly attached to the porphyrine π system in Chl *a* at positions 2, 7, and 12 (Figure 1). We anticipate that the three tensors **A**, **B**, and **C** result from the methyl protons of a Chl *a* molecule. A comparison with the well-understood Chl $a^{+\bullet}$[38,74,75] supports such an assignment (see Table 3).

The small hf anisotropy of the equivalent CH_3 group protons leads to large intensities of the lines.[71] The tensors are axially symmetric to good approximation. The tensor axis attributed to the largest principal value (A_3) is lying along the C−CH_3 bond direction. A deviation may occur due to the next-neighbor spin densities. However, semiempirical molecular orbital calculations[75,77] indicate that these deviations are rather small ($\leq \pm 10°$).[38] This should therefore not affect the assignment of the three methyl proton tensors in $P_{700}^{+\bullet}$. In the following, we assume that the tensor axes are parallel to the bond directions.

Figure 9 shows the angles between the methyl bonds and the crystallographic *c* axis. The angles determined from ENDOR with respect to the *c* axis are found on the inner circle (accuracy ±5°). The assignment of these experimental angles to specific positions in a Chl *a* molecule is based on a comparison with the molecular geometry of ethyl chlorophyllide *a* as determined from an X-ray structure analysis.[78] Ethyl chlorophyllide *a* is planar to a good approximation. Angles between methyl bonds and the molecular *x* and *y* axes, calculated from the X-ray structure, are given on the outer circle in Figure 9.

By specific deuteration experiments, the largest of the three hfc's of the Chl *a* cation radical has been assigned to the methyl protons at position 12.[74] This assignment has been supported by the investigation of a series of chlorophyll derivatives;[38] it also holds for the BChl *a* cation radical.[55,79] It can therefore be safely assumed that the largest of the three tensors **A** determined

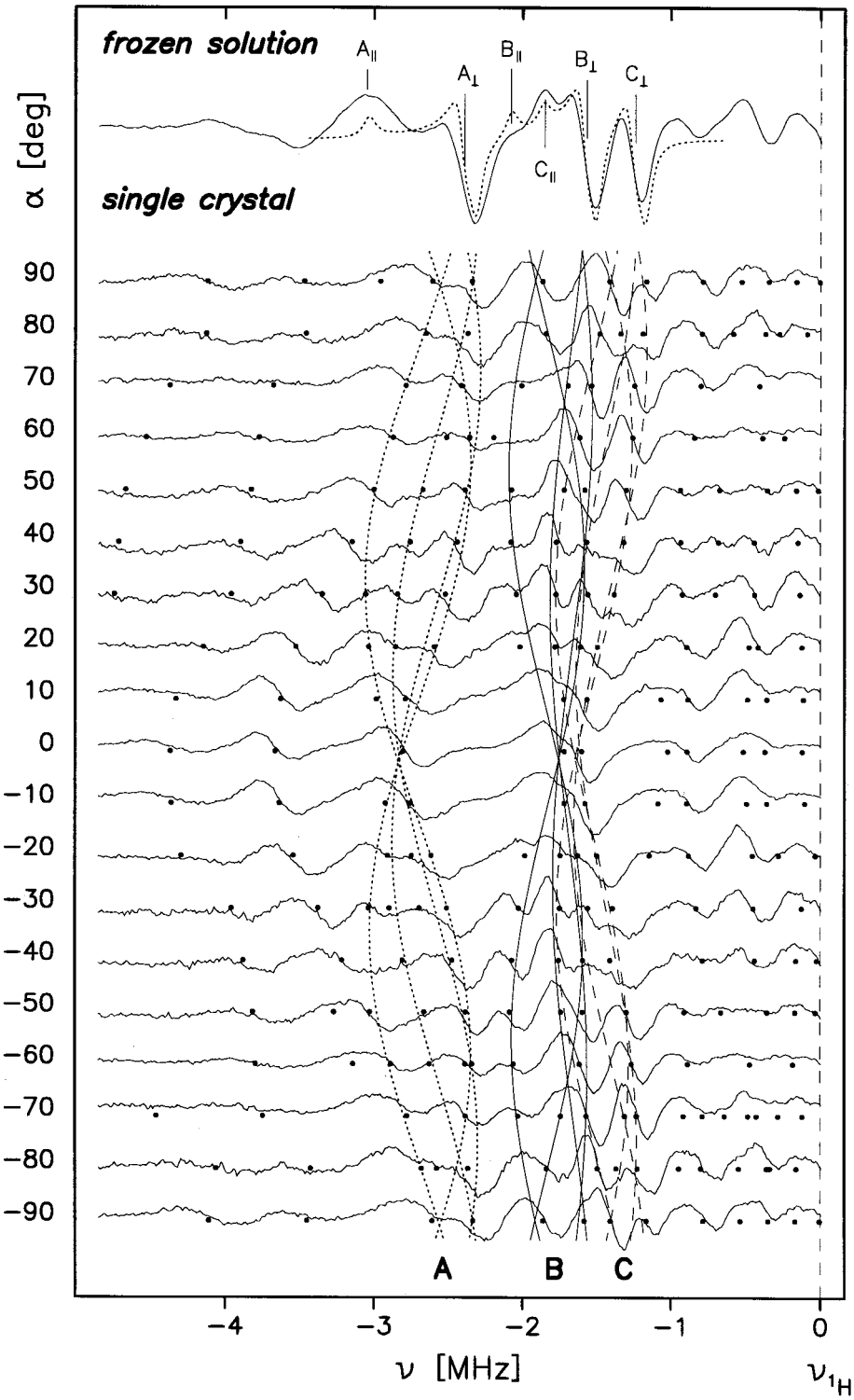

Figure 7. Complete set of ENDOR spectra for rotation of a PS I single crystal perpendicular to its crystallographic *c* axis. Only the low-frequency part (below $\nu_{^1H}$) is shown. Deconvoluted line positions are represented by black dots (•). The rotation patterns **A**, **B**, and **C** calculated from the hfc tensors given in Table 2 are included. The theoretical ENDOR powder spectrum resulting from the methyl proton hfc tensors of Table 2 was simulated[55] and is shown in comparison with the experimental spectrum of $P_{700}^{+\bullet}$ in frozen solution (top). The assumption of purely axial hfc tensors was used, which yields reasonable estimates for the methyl hfc tensor values.[72] The positions of the respective $A_{\|}$ and $A_{\perp}$ values are indicated for **A**, **B**, and **C**: (**A**) 6.10, 4.78, and 5.22 MHz; (**B**) 4.16, 3.14, and 3.48 MHz; (**C**) 3.70, 21.48, and 2.89 MHz (values are given as ($A_{\|}$, $A_{\perp}$, and A_{iso}). For experimental parameters, see Figure 5a.

for $P_{700}^{+\bullet}$ also belongs to the methyl protons at position 12 in the Chl *a* cation radical. The angle between the corresponding methyl bond direction and the *c* axis is 33°.

The X-ray structure analysis of ethyl chlorophyll *a* yields an angle of 176° between the methyl ($C-CH_3$) bond directions at molecular positions 12 and 2. Therefore, the angle between the methyl bond at position 2 and the crystallographic *c* axis will be either (a) 29° or (b) 37°. If the measured angle of 30° between the orientation of the A_3 axis of tensor **C** and the *c* axis is considered, possibility (a) is the most likely one (Figure 9). In addition, the assignment of hfc tensor **B** (position 7) to the methyl protons at position 2 can be excluded, since the angle

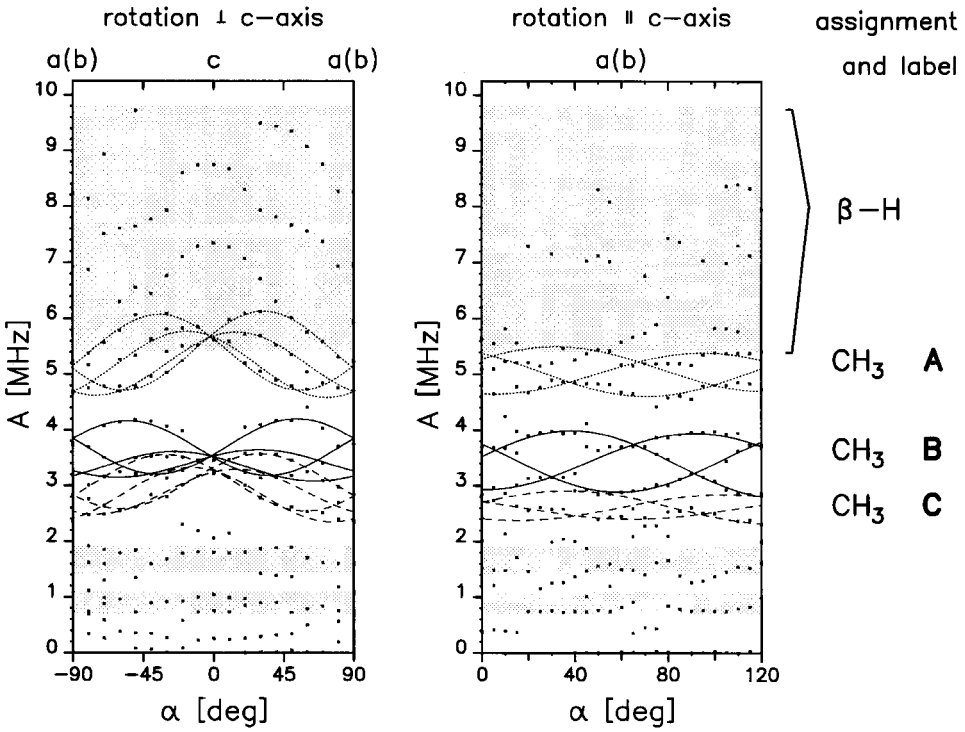

Figure 8. Experimentally determined hf splittings (black dots), calculated rotation patterns for three different hfc tensors (dotted, dashed, and solid lines), and ranges of additional prominent hfc's (shaded areas). The rotation patterns shown here are fits to the experimental hfc's (some of the corresponding spectra are shown in Figure 5). Assignments are indicated on the right.

TABLE 2: Principal Hyperfine Tensor Values [MHz], Tensor Orientations, and Assignments of Methyl Protons in $P_{700}^{+\bullet}$ of *Synechococcus elongatus*

	hfc tensor values[a]			isotropic hfc	orientation[b]	
tensor	A_1	A_2	A_3	A_{iso}	γ	assignment[c]
A	4.70	4.65	6.10	5.15	33°	12
B	3.15	2.80	4.20	3.40	54°	7
C	2.55	2.35	3.55	2.80	30°	2

[a] For assignment of the experimentally determined hfc's to the individual hfc tensor diagonal element, A_1, A_2, and A_3, see text. The values given were evaluated from the fit parameters, errors ±100 kHz. [b] γ denotes the angle between the A_3 principal tensor axis and the crystallographic *c* axis (see text and Figure 6), error ±5°. [c] All three hfc tensors are assigned to the methyl groups of one single chlorophyll molecule (see text). For numbering of molecular positions, see Figure 1.

of 54° (±5°) between its A_3 axis and the *c* axis fits neither case a nor case b. The crystallographic angle between the methyl bond directions of positions 12 and 7 is 94.7°. This is close to the value of 33° + 54° = 87° deduced from the respective hfc tensor values (Figure 9). In conclusion, hfc tensor **C** is assigned to the protons of the methyl group at position 2 of the spin-carrying Chl *a* molecule in $P_{700}^{+\bullet}$ and the remaining hfc tensor **B** to the methyl protons at position 7 of this Chl *a* molecule.

Orientation of the Spin-Carrying Chl a in the PS I Complex. We have determined the orientation of the spin-carrying Chl *a* in $P_{700}^{+\bullet}$ relative to the crystallographic *c* axis. This *c* axis is essentially parallel to the pseudo-C_2 axis of the PS I protein.[8,53] For convenience, only the Chl *a* molecule located at site 1 of the crystal unit cell is discussed. All conclusions made in the following are also valid for the Chl *a* molecules on the other five symmetry-related sites of the unit cell.

In addition to the situation depicted in Figure 9, there are three other possible symmetry-equivalent orientations of the spin-carrying Chl *a* molecule. The four possible orientations of

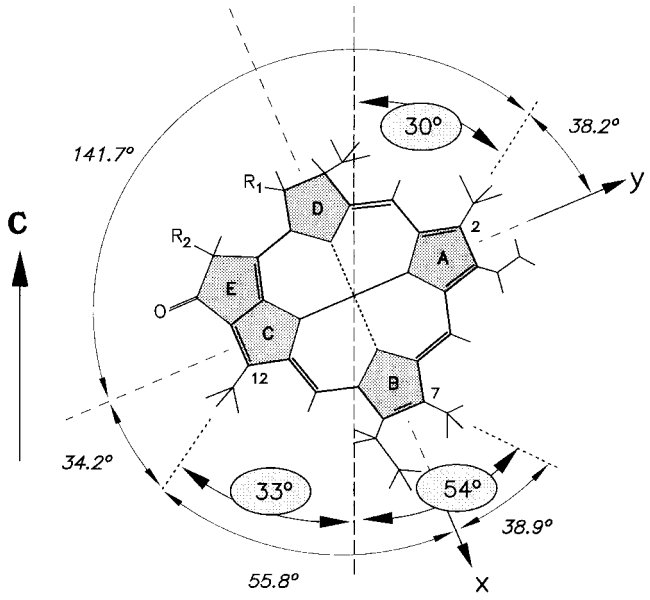

Figure 9. Comparison of geometrical results from the X-ray structure analysis[78] of ethyl chlorophyllide *a* and from ENDOR on $P_{700}^{+\bullet}$ in PS I single crystals. The outer circle gives angles (in italics) between C−CH_3 bonds and the molecular *x* (*y*) axes determined for the ethyl chlorophyllide *a* molecule. On the inner circle, the angles between the C−CH_3 bonds and the crystallographic *c* axis are given which were measured for the spin-carrying Chl *a* half of $P_{700}^{+\bullet}$ in the PS I single crystal. The orientation of the *c* axis is indicated by the dashed vertical line.

the C−CH_3 bond direction described by angle γ (Figure 6) relative to the *c* axis are γ, $-\gamma$, 180° − γ, and 180° + γ. Since the phytyl side chain of the Chl *a* should point toward the stromal side of the PS I complex, i.e., into the interior of the protein as in the purple bacterial RC, the two cases 180° ± γ can be safely excluded (cf. Figure 2). This leaves us with the two orientations ±γ.

TABLE 3: ^{1}H HFS Data [MHz] of Chl $a^{+\bullet}$ and of $P_{700}^{+\bullet}$ in PS I Determined by ENDOR Spectroscopy in Frozen Solutions

Chl $a^{+\bullet}$	$P_{700}^{+\bullet}$		$P_{700}^{+\bullet}$ comparison with literature[b]				
CH_2Cl_2/THF[75] $T = 200$ K	*Synechococcus elongatus*[c] $T = 100$ K	assignment[a] position (group)	*Chlorella vulgaris*[32] $T = 100$ K	spinach[13] $T = 77$ K	spinach[36] $T = 123$ K	*Scenedesmus obliquus*[39] $T = 210$ K	spinach[65] $T = 10$ K[d]
10.3	9.6	17,18 (βH)	−	−	−	−	−
10.1	7.7	17,18 (βH)	−	7.5 (−)	7.5 (−)	7.5 (17,18)	7.2 (17,18)
7.1	5.3	12^1 (CH_3)	5.3 (17,18)	5.2 (−)	5.3[e] (12^1)	5.0 (12^1)	5.6 (12^1)
3.0[f]	3.5	7^1 (CH_3)	3.6 (12^1)	3.4 (−)	3.3 (7^1)	3.3 (2^1,7^1)	3.4 (7^1)
3.0[f]	2.9	2^1 (CH_3)	−	2.7 (−)	2.6 (2^1,8^1)	2.8 (8^1)	2.6 (2^1)
2.2[g]	1.8	n.a.	1.7 (7^1)	−	1.9 (8^1)	1.4 (3^2,13^2)	1.8 (8^1)
0.6	0.8	n.a	−	−	0.8 (3^1,m)	0.7 (3^1,m)	0.9 (m)

[a] For numbering of positions, see Figure 1. The assignment is based on the single-crystal ENDOR spectra obtained in this work. For possible assignments of the two small hfc's, see text; n.a. = not assigned. [b] The numbers in brackets give the assignment of the respective hfc's made in the original references, m = methine (positions 5, 10, and 20). [c] This work. Note that for the CH_3 protons, the isotropic hfc's are given and not the individual tensor components (cf. powder ENDOR data in Table 1) for better comparison with the average powder ENDOR data found in the literature. [d] Note that these data were obtained at very low temperature, at which some of the hfc's might be influenced by dynamical effects (see text); this is particularly true for the hfc at position 12^1. [e] The authors gave two hfc's (5.0 and 5.9 MHz) that we assign to the tensor components $A_\perp$ and $A_\parallel$ of the 12^1 CH_3 protons. The value of 5.3 MHz is the respective isotropic hfc. [f] These hfc's are split in 3-acetyl Chl $a^{+\bullet}$,[38] showing that they are degenerate in Chl $a^{+\bullet}$; the use of CH_2Cl_2/CH_3OH as solvent mixture did not significantly change the hfc's.[75] [g] This hfc has a negative sign; it is hard to detect in frozen solutions.[38] Note that the data given here were obtained in liquid (isotropic) solution.[75]

Assignment of Additionally Observed hfc's. Additional lines are found in the ENDOR spectra (see Figures 7 and 8) that are clearly related to each other. However, the angular dependence of the hf splittings could not be completely followed, which make an analysis and assignment of the hfc's difficult.

Several of these lines fall into the range of the large hfc's above 6 MHz. They show a significant angular variation over a range of 5.5−8.8 MHz (Figure 8). In particular, in the case of the rotation perpendicular to the *c* axis, the respective ENDOR lines are quite pronounced. The lower limit of these hfc's is difficult to estimate because they partially overlap with the rotation pattern of the largest methyl group hf tensor of position 12. On the basis of the magnitude of the hf splittings and a comparison with the hfc's of Chl $a^{+\bullet}$,[21,38,74] these lines are assigned to the β-protons on ring D (positions 17 and 18; see Figure 1) of the spin-carrying Chl *a* in $P_{700}^{+\bullet}$. This is supported by the smaller intensity of these lines compared with that of the methyl groups. Furthermore, the magnitude of their anisotropy is similar to that of the β-protons of the primary donor cation radical $P_{865}^{+\bullet}$ in purple bacterial RCs.[22]

A second class of lines shows hfc values below 2 MHz. They are quite intense and do not exhibit a clear dependence on the rotational angle, in particular, in the case of rotation around the *c* axis. In principle, several assignments are possible for these small hfc's:

(i) According to ENDOR experiments[55,42,38] and MO calculations[38] on Chl $a^{+\bullet}$, various hf tensor components of protons attached to the macrocycle could be responsible for these couplings, i.e., CH_2 (position 8^1, 17^1), CH_3 (position 18^1), α-protons (position 5, 10, 20), vinyl-protons (position 3^1, 3^2), and the H at position 13^2. On the basis of theoretical estimates of these couplings (see Table 4 in ref 38), none of these interactions can definitely be excluded to contribute to this range.

(ii) A contribution of protons from the surrounding amino acids (matrix) is also possible, in particular, to the smaller hf splitting in the ENDOR spectra.[16]

(iii) Another possibility is an assignment of the small hf splittings to protons of the chlorophyll from the other dimer half of $P_{700}^{+\bullet}$ (e.g., to the intense methyl proton resonances at positions 12^1, 7^1, and 2^1). To investigate this possibility, we have scaled down the individual CH_3 tensor components from Table 2 by factors of 0.25−0.30[80] and could satisfactorily simulate the rotation patterns. This shows that such an assignment can also not be excluded from the interpretation of the $P_{700}^{+\bullet}$ single-crystal ENDOR spectra.

In conclusion, it is likely that the lines observed in this region ($A < 2$ MHz) are a superposition of hfc's from different sources. This makes a unique assignment of these line pairs in the spectra very difficult and thus prevents a possible determination of small hf splittings from the putative second half of the P_{700} dimer.

Discussion

Electronic Structure of $P_{700}^{+\bullet}$. The ^{1}H hfc's of $P_{700}^{+\bullet}$ from various organisms published in the literature[13,32,36,39,65] are compared with our data from *S. elongatus* and with the isotropic hfc's of Chl $a^{+\bullet}$ in organic solvents[75] in Table 3. To allow a convenient comparison, we calculated isotropic hfc's from the hf components ($A_\parallel$,$A_\perp$) of the three methyl group tensors in the powder ENDOR spectra of $P_{700}^{+\bullet}$; for the other couplings, effective values are given. The comparison clearly shows that the experimental values for *S. elongatus* are fully consistent with those determined from other organisms. However, differences in the assignments of the lines to specific protons led to different interpretations of the spin densitiy distribution of $P_{700}^{+\bullet}$ in the past. These assignments are also included in Table 3. The ENDOR work on PS I single crystals presented here and discussed below finally solves most of the assignment problems.

All experiments performed in the past failed to detect the weak powder ENDOR lines of the largest β-proton coupling. A comparison of the smaller β-proton hfc measured by different authors, however, shows a satisfying agreement (Table 3). A complete determination of the β-proton hfc tensors has not been possible from our single-crystal spectra (cf. also ref 81). However, this is not a serious problem for the determination of the electronic structure of $P_{700}^{+\bullet}$, since the β-protons are not good probes for the spin density in the chlorophyll macrocycle. This is due to the fact that the geometry of ring D in $P_{700}^{+\bullet}$ (Figure 1) and thus the dihedral angles for the β-protons, which determine the hfc's,[58] are unknown. Therefore, the electron spin density of the neighboring π center cannot be obtained directly from the hf coupling.

The methyl proton hfc's could be fully analyzed in the single-crystal ENDOR spectra (see Table 2). In the following, we will discuss these hfc's and compare them with previous experiments performed on $P_{700}^{+\bullet}$ in frozen PS I solutions. The comparison is summarized in Table 3. Norris et al.[32] assigned the hfc of 3.6

MHz to the largest methyl proton hfc of $P_{700}^{+\bullet}$ and the hfc of 5.3 MHz to the β-protons (positions 17,18); no larger hfc's could be detected in this work. Our results show that the hfc's of 3.6 and 5.3 MHz are due to the methyl protons at positions 7^1 and 12^1 of the spin-carrying Chl *a*. The simple special pair model[31,32] resulting from this incorrect assignment, which was based on a halving of the monomer hfc's in the dimer, must therefore be considered inadequate to describe the electronic structure of $P_{700}^{+\bullet}$.

In the recent work of Rigby et al.,[65] the hf data (Table 3) were interpreted by a comparison with the monomeric Chl *a* cation radical. The authors postulated a dimeric model for $P_{700}^{+\bullet}$ with an asymmetric spin density distribution over the chlorophyll halves of about 3:1. No hfc's were assigned to a second dimer half in this work. The authors could therefore not rigorously exclude the possibility that $P_{700}^{+\bullet}$ is a modified Chl $a^{+\bullet}$ monomer.[65] Furthermore, the experiments were performed at very low temperatures ($T = 10$ K). Thus, the obtained hf splittings must be interpreted with caution, since at such low temperatures some of the motional processes in the radical are frozen out as discussed above. This results in altered values of the related hfc's and leads to misleading conclusions about the spin density distribution (see discussion of Figure 4).

The assignment of the prominent methyl proton hfc's to molecular positions 2^1, 7^1, and 12^1 and of the β proton hfc to positions 17/18 in our work agrees with the assignments of O'Malley and Babcock.[36] The value of 5.9 MHz, which was interpreted by these authors as being due to the β-protons at positions 17/18, turned out to be the $A_{||}$ (A_3) hfc component of the 12^1 methyl group protons. On the basis of their experimental ^{1}H ENDOR data and MO theoretical results, O'Malley and Babcock[36] and, more recently, Mac et al.[45] proposed that $P_{700}^{+\bullet}$ is a monomeric Chl $a^{+\bullet}$ with a spin density distribution different from that found in organic solvents. The authors' model is based on earlier MO calculations[37] which indicated that in chlorophyll radical cations the doublet ground state, D_0, and first excited state, D_1, are energetically close to each other. Caused by ligation effects and/or conformational changes of the macrocycle, these states might mix and lead to different hybrid orbitals carrying the spin for monomeric Chl $a^{+\bullet}$ *in vitro* (organic solvents) and for a Chl *a* cation radical forming $P_{700}^{+\bullet}$ in the PS I protein. However, this model fails in the estimation of the most prominent methyl proton hfc value for position 12^1 in $P_{700}^{+\bullet}$. Furthermore, the postulated admixture of D_1 in $P_{700}^{+\bullet}$ with higher spin density at noncarbon atoms (N,O) showing higher spin−orbit coupling constants[82] should result in a larger *g* value. This has not been found experimentally; the *g* value is 2.0025(1) for both $P_{700}^{+\bullet}$ and Chl $a^{+\bullet}$.[21] Another problem with this model is the estimation of the nitrogen hfc's. Following the theoretical predictions of the "orbital mixing" model, the nitrogen spin density should be positive in $P_{700}^{+\bullet}$, and the nitrogen hfc's should be significantly increased compared with those of Chl $a^{+\bullet}$ in solution. In contrast to that, ^{15}N ENDOR and ESEEM experiments[42,81] clearly gave negative nitrogen spin densities in $P_{700}^{+\bullet}$. Furthermore, no pronounced change of the magnitudes of the nitrogen hfc's was detected for ^{15}N Chl $a^{+\bullet}$ and ^{15}N $P_{700}^{+\bullet}$.[42,43]

The orbital mixing model has recently been probed by investigating chlorophyll cation radicals with a number of different substituents.[38] No indication has been found for the validity of this model. It has been postulated[38] that most of the problems encountered with the spectroscopy of Chl *a* cation radicals are probably due to aggregation phenomena in solution. For $P_{700}^{+\bullet}$, such problems do not exist, since the radical is bound in a protein pocket. The ENDOR resonances can be saturated without problems, leading to good ENDOR intensities. This would not be the case for a substantial mixing of the doublet ground and first excited state. On the basis of the above given arguments, the orbital mixing model seems to be inadequate to explain the changes of hfc's in $P_{700}^{+\bullet}$ compared with those of Chl $a^{+\bullet}$ in organic solvents.

A decision about the monomeric or dimeric nature of $P_{700}^{+\bullet}$ should be possible on the basis of the measured and assigned hyperfine coupling constants of $P_{700}^{+\bullet}$. The assignment of a dimeric species, however, requires the detection of hfc's from both dimer halves, as shown for the primary donors in purple bacterial reaction centers.[22] Unfortunately, a clear assignment of experimental ^{1}H hfc's to a second dimer half has not been achieved so far for $P_{700}^{+\bullet}$, which makes a final decision difficult. A different approach to estimate the nature of the spin density distribution in $P_{700}^{+\bullet}$ is to compare the hfc data with those of monomeric Chl $a^{+\bullet}$ in organic solvents. This is, however, not very reliable, since the electronic structure of Chl $a^{+\bullet}$ is influenced by solvent, counterion, and temperature, leading to a variation of the hyperfine coupling constants and of the EPR line width (for a compilation of data, see Table 3 in ref 21). In earlier work[38,74,75] performed on Chl $a^{+\bullet}$ and on various differently substituted and labeled Chl $a^{+\bullet}$ species,[38] the three methyl groups at positions 12^1, 7^1, and 2^1 could be safely assigned; one data set is shown in Table 3. In $P_{700}^{+\bullet}$, the respective values for A_{CH_3} (12^1) and A_{CH_3} (2^1) are reduced, whereas that for A_{CH_3} (7^1) is increased. This indicates a redistribution of spin density in the Chl macrocycle. On the basis of a comparison of the sum of the three assigned methyl hfc's in $P_{700}^{+\bullet}$ (Tables 2,3) and those in Chl $a^{+\bullet}$ (Table 3), it can be argued[81] that $\geq$85% of the spin is located on the "spin-carrying" chlorophyll molecule; the rest ($\leq$15%) is probably spread out onto other positions that do not carry magnetic nuclei, to protein ligands or to the putative second Chl half.

The primary donor cation radicals $P_{865}^{+\bullet}$ in *Rb. sphaeroides*[22] and $P_{960}^{+\bullet}$ in *Rps. viridis*[26] are known to be bacteriochlorophyll dimers. In both cases, the ratio of the sum of spin densities, derived from the CH_3 hfc's, for the two dimer halves yielded values close to 2:1. For the primary donor in *Rb. sphaeroides*, it has been shown that the spin density distribution in $P_{865}^{+\bullet}$ reacts in a very sensitive way to temperature and type of detergent[66] and, in particular, to mutations that change the amino acids interacting with the primary donor.[83,27] In all cases, a shift of spin density between the two halves of the dimer is observed. This has been explained[66,83] by the special electronic properties of the dimeric species. In recent work,[46,48] we exchanged amino acids in the vicinity of the primary donor in PS I of the green algae *Chlamydomonas* (*C.*) *reinhardtii*. In this species, $P_{700}^{+\bullet}$ shows hyperfine coupling constants that are very similar to those of *S. elongatus* described in this work.[81] An exchange of histidine H(B656) in the PsaB protein of *C. reinhardtii* to various other amino acids affects the hfc's and the redox potential and shows that this residue is a ligand of the spin-carrying half of $P_{700}^{+\bullet}$.[48] In the respective ENDOR spectra, an increase of the large methyl hfc at position 12^1 is observed, but a concomitant decrease of the magnitude of the small hfc's could not be detected. This is in contrast to the findings for the primary donor $P_{865}^{+\bullet}$ in the purple bacterial RC. Exchange of the symmetry-related histidine H(A676) in the PsaA protein of *C. reinhardtii*, the putative ligand of the second Chl *a* half of the dimer forming P_{700}, showed no effect on the spin density distribution.[48] This,

together with other biophysical experiments on these mutants,[48] indicated that the spin density is essentially localized on one Chl half of $P_{700}^{+\bullet}$.

X-ray crystallography has shown that P_{700} is a closely related Chl dimer.[7,8] The two halves are excitonically coupled, as shown by optical techniques.[5,84] The coupling was estimated for P_{700} to be much weaker than that of P_{865}[85,86] or P_{960}[87] in purple bacterial RCs. This reflects the smaller transition moment of Chl *a* compared to that of BChl *a* and, in addition, could also be due to a different geometry of the two chlorophylls forming P_{700}, which is indeed indicated in the recent X-ray structure.[54] This could, in principle, lead to an asymmetric spin density distribution in $P_{700}^{+\bullet}$.

Furthermore, the free energy of the two chlorophyll halves of P_{700} could be quite different. In the most recent X-ray crystallographic work at 2,5 Å resolution,[54] it was shown that P_{700} is made up from one Chl *a* molecule and one Chl *a*′ molecule, the C13[2] epimer of Chl *a*. Chl *a*′ and Chl *a* are bound to protein subunits PsaA and PsaB, respectively. On the basis of the site-directed mutagenesis experiments,[48] it could be shown that the chlorophyll bound to PsaB, i.e., the Chl *a*, is carrying the spin. Obviously, interactions with the protein surrounding lower the energy of the Chl *a*′ half below that of Chl *a* so that the latter is oxidized in the photoprocess. Such effects have been observed in mutants of *Rb. sphaeroides* with specific alterations of hydrogen bonds to the primary donor P_{865}.[83] FTIR has detected a strong H bond to the 13[1] carbonyl oxygen of the non-spin-carrying half of P_{700},[51] i.e., to the Chl *a*′ molecule. This is in agreement with the assumption that Chl *a* is the active (oxidized) half of P_{700}. Hydrogen bonds to the Chl *a*′ have indeed been detected in the most recent X-ray crystallographic structure, whereas there are no H bonds to the Chl *a* half of P_{700}.[54] So far, it is unknown how much spin density is actually delocalized on the Chl *a*′ half of this dimer. The recent detection of a broad mid-IR band near 3300 cm^{-1},[51] which is assigned to an electronic transition in a dimeric species, might indicate some charge delocalization in $P_{700}^{+\bullet}$. Molecular orbital model calculations using different Chl model dimers, also including Chl *a*′, are currently carried out in our laboratory with the aim of relating the dimer geometry to the spin density distribution. This approach is also expected to yield insight into a possible spin density redistribution caused by interaction with surrounding amino acids or other ligands of $P_{700}^{+\bullet}$ (cf. ref 88).

Geometry of the Primary Donor. The ENDOR experiments on single crystals of PS I presented here yield geometrical information concerning the spin-carrying Chl *a* molecule in $P_{700}^{+\bullet}$ via the determination of the hf tensor axes (see Table 2). The results achieved by EPR on the triplet state of P_{700}[5,89] are consistent with our structural model of $P_{700}^{+\bullet}$.[90] It is found that the orientation of this molecule with respect to the C_2 pseudosymmetry axis of the PS I protein is similar to that of the almost symmetrically positioned BChl halves constituting the primary donors P_{865} and P_{960} in the RC's of *Rb. sphaeroides* and *Rps. viridis*,[19] respectively. In these RC's, the analogous C_2 pseudosymmetry axis relates the two cofactor branches to each other and runs through the center of the line connecting the two Mg atoms of the BChl molecules forming the dimer. The angles[91] between the bonds of the respective methyl groups at position 12 and the C_2 axis are 37° and 34° in case of the two structures of *Rb. sphaeroides*[92,93] and 36° in *Rps*. viridis;[94] in PS I, it is 33° (Table 2). Similar to the situation found in P_{700}, the C_2 axis is running parallel to the average molecular plane of the BChl molecules in the purple bacterial RC's. Thus, the orientation of the spin-carrying half of P_{700} is very similar to that of the symmetrically positioned BChl molecules both in P_{865} and P_{960} of these RCs. The equivalent orientation of the bacteriochlorophylls in the primary donor of purple bacterial RCs and one chlorophyll half of P_{700} in PS I suggests that a special geometry might be essential for the primary event of light-induced charge separation and has therefore been conserved in evolution.[95]

Summary and Conclusion

In this work, the primary donor cation radical $P_{700}^{+\bullet}$ was investigated for the first time by EPR/ENDOR techniques in PS I single crystals. The ^1H hfc tensors of three CH_3 groups were evaluated and assigned to one single Chl *a* molecule. This work on $P_{700}^{+\bullet}$-together with our recent results on genetically modified PS I[48]-indicates that this species is essentially a "spin monomer", although the X-ray crystallographic analysis of PS I single crystals clearly shows the existence of two chlorophylls constituting the structure of the primary donor.[7−9] This finding is in agreement with the results from other laboratories.[34,36,45]

The lack of spin density delocalization on the second dimer half indicates that either the coupling of the two halves is small or the energetic difference is rather large. A weak coupling is indicated by the much smaller excitonic interaction of P_{700} compared to that of the primary donors P_{865} and P_{960} in purple bacterial reaction centers. An energetic difference is indicated by the "heterodimeric character" of P_{700}, which is made up of one Chl *a* molecule and one Chl *a*′ molecule (see ref 54). The X-ray crystallographic results at 2.5 Å resolution[54] show a different surrounding of the two chlorophylls, which is supported by FTIR spectroscopic data.[51] This leads to further energetic difference between the dimer halves. The strongly reduced redox potential of $P_{700}/P_{700}^{+\bullet}$ compared with that of Chl *a*/Chl $a^{+\bullet}$ still remains a puzzle. This effect cannot be explained by the formation of a dimer, since the charge in $P_{700}^{+\bullet}$ is mainly localized on only one chlorophyll in this species, as clearly shown in this work. One possibility is that the altered redox potential is caused by the special electrostatic environment of the primary donor. Another challenging explanation would be the formation of a chlorophyll *a* enol, as suggested earlier by Wasielewski et al.[35]

The C_2 pseudosymmetry axis of the PS I protein-which is parallel to the crystallographic *c* axis-lies in the molecular plane of the spin-carrying Chl *a*. The angle between the bond of the methyl group at position 12 of this molecule and the C_2 axis is 33°; for the methyl groups at molecular positions 7 and 2, the respective angles are 54° and 30°. From these data, the orientation of the spin-carrying Chl *a* molecule in $P_{700}^{+\bullet}$ in PS I was determined. The Chl *a* is oriented similarly to the BChl molecules forming the primary donor in the RC of purple bacteria. This indicates a significant structural similarity of the primary donors in these RCs and PS I. This similarity could have an evolutionary origin.[95] It is also interesting to speculate whether such an arrangement is required for maximum efficiency of P_{700} as a light trap, for optimum electron transfer in the reaction center, and/or for an effective reduction of $P_{700}^{+\bullet}$ by the soluble electron donor proteins from the lumenal side.

In this context, the structure and unusual redox properties of the primary donor in PS II, P_{680}, are very interesting. It has been proposed that P_{680} is also a Chl *a* species but with a rather large distance of the chlorophyll halves (center-to-center distance, 10−11 Å).[96,97] This would lead to a vanishing excitonic coupling, as is observed experimentally and, in the cation radical $P_{680}^{+\bullet}$, to a clear localization of the spin density on one chlorophyll molecule. This is indeed indicated in recent EPR

and ENDOR work performed on $P_{680}^{+\bullet}$ in special PS II preparations.[65,98] For the work on the electronic structure of the primary donors in photosynthetic systems to be completed, further experiments on $P_{680}^{+\bullet}$ are in progress.

Acknowledgment. We thank E. Schlodder and F. Lendzian (Max-Volmer-Institut für Biophysikalische Chemie und Biochemie, Technische Universität Berlin) for many helpful discussions concerning the data interpretations and modeling of P_{700}. P. Jordan, N. Krauss, and W. Saenger (Institut für Chemie, Freie Universität Berlin) are gratefully acknowledged for communicating details of the recent X-ray structure analysis of PS I single crystals prior to publication. This work has been supported by Deutsche Forschungsgemeinschaft (Sfb 312, TP A3 and A4; Sfb 498, TP A1 and C5) and Fonds der Chemischen Industrie (to W.L. and P.F.).

References and Notes

(1) Golbeck, J. H. In *Molecular Biology of Cyanobacteria*, *Adv. Photosynth. 1*; Bryant, D. A., Ed.; Kluwer Academic Publishers: Dordrecht, The Netherlands, 1994; pp 179−220.

(2) Chitnis, P. R.; Xu, Q.; Chitnis, V. P.; Nechushtai, R. *Photosynth. Res.* **1995**, *44*, 23−40.

(3) Chitnis, P. R. *Plant Physiol.* **1996**, *111*, 661−669.

(4) Fromme, P. *Curr. Opin. Struct. Biol.* **1996**, *3*, 473−484.

(5) Brettl, K. *Biochim. Biophys. Acta* **1997**, *1318*, 322−373.

(6) Fromme, P.; Witt, H. T. *Biochim. Biophys. Acta* **1998**, *1365*, 175−184.

(7) Krauss, N.; Schubert, W.-D.; Klukas, O.; Fromme, P.; Witt, H. T.; Saenger, W. *Nature Struct. Biol.* **1996**, *3*, 965−970.

(8) Schubert, W.-D.; Klukas, O.; Krauss, N.; Saenger, W.; Fromme, P.; Witt, H. T. *J. Mol. Biol.* **1997**, *272*, 741−769.

(9) Klukas, O.; Schubert, W.-D.; Jordan, P.; Krauss, N.; Fromme, P.; Witt, H. T.; Saenger, W. *J. Biol. Chem.* **1999**, *274*, 7361−7367.

(10) Klukas, O.; Schubert, W.-D.; Jordan, P.; Krauss, N.; Fromme, P.; Witt, H. T.; Saenger, W. *J. Biol. Chem.* **1999**, *274*, 7351−7360.

(11) Joliot, P.; Joliot, A. *Biochemistry* **1999**, *38*, 11130.

(12) *Biophysical Techniques in Photosynthesis*; Amesz, J.; Hoff, A. J., Eds.; Kluwer Academic Publishers: Dordrecht, The Netherlands, 1996; Vol. 2.

(13) Hoff, A. J. *Phys. Rep.* **1979**, *54*, 75−200.

(14) Hoff, A. J. *Biophys. Struct. Mech.* **1982**, *8*, 107−150.

(15) Lubitz, W.; Lendzian, F. In *Biophysical Techniques in Photosynthesis*; Amesz, J., Hoff, A. J., Eds.; Kluwer Academic Publishers: Dordrecht, The Netherlands, 1996; Vol. 3; pp 255−275.

(16) Kurreck, H.; Kirste, B.; Lubitz, W. *Electron Nuclear Double Resonance Spectroscopy of Radicals in Solution - Applications to Organic and Biological Chemistry*; VCH Publishers: Deerfield Beach, FL, 1988.

(17) Möbius, K.; Lubitz, W. In *Biological Magnetic Resonance*; Berliner, L. J., Reuben, J., Eds.; Plenum Press: New York, 1987; Vol. 7, pp 129−247.

(18) Dikanov, S. A.; Tsvetkov, Y. D. *Electron Spin-Echo Envelope Modulation (ESEEM) Spectroscopy*; CRC Press: Boca Raton, FL, 1992.

(19) Lancaster, C. R. D.; Ermler, U.; Michel, H. In *Anoxygenic Photosynthetic Bacteria*; Blankenship, R. E., Madigan, M. T., Bauer, C. E., Eds.; Kluwer Academic Publishers: Dordrecht, The Netherlands, 1995; pp 503−526.

(20) Watanabe, T.; Kobayashi, M. In *Chlorophylls*; Scheer, H., Ed.; CRC Press: Boca Raton, FL, 1991; pp 287−364.

(21) Lubitz, W. In *Chlorophylls*; Scheer, H., Ed.; CRC Press: Boca Raton, 1991; pp 903−944.

(22) Lendzian, F.; Huber, M.; Isaacson, R. A.; Endeward, B.; Plato, M.; Bönigk, B.; Möbius, K.; Lubitz, W.; Feher, G. *Biochim. Biophys. Acta* **1993**, *1183*, 139−160.

(23) Feher, G. *J. Chem. Soc., Perkin Trans.* **1992**, *2*, *11*, 1861−1874.

(24) Käss, H.; Rautter, J.; Bönigk, B.; Höfer, P.; Lubitz, W. *J. Phys. Chem.* **1995**, *99*, 436−448.

(25) Davis, I. H.; Heathcote, P.; MacLachlan, D. J.; Evans, M. C. W. *Biochim. Biophys. Acta* **1993**, *1143*, 183−189.

(26) Lendzian, F.; Lubitz, W.; Scheer, H.; Hoff, A. J.; Plato, M.; Tränkle, E.; Möbius, K. *Chem. Phys. Lett.* **1988**, *148*, 377−385.

(27) Artz, K.; Williams, J. C.; Allen, J. P.; Lendzian, F.; Rautter, J.; Lubitz, W. *Proc. Natl. Acad. Sci. U.S.A.* **1997**, *94*, 13582−13587.

(28) Rautter, J.; Lendzian, F.; Lin, X.; Williams, J. C.; Allen, J. P.; Lubitz, W. In *The Reaction Center of Photosynthetic Bacteria, Structure and Dynamics*; Michel-Beyerle, M.-E., Ed.; Springer: Berlin, 1996; pp 37−50.

(29) Döring, G.; Bailey, J. L.; Kreutz, W.; Weikard, J.; Witt, H. T. *Naturwissenschaften* **1968**, *55*, 219−220.

(30) Norris, J. R.; Druyan, M. E.; Katz, J. J. *J. Am. Chem. Soc.* **1973**, *95*, 1680−1682.

(31) Norris, J. R.; Scheer, H.; Druyan, M. E.; Katz, J. *J. Proc. Natl. Acad. Sci. U.S.A.* **1974**, *71*, 4897−4900.

(32) Norris, J. R.; Scheer, H.; Katz, J. J. *Ann. N.Y. Acad. Sci.* **1975**, *244*, 260−280.

(33) Wasielewski, M. R. In *Light Reaction Path of Photosynthesis*; Fong, F. K., Ed.; Springer-Verlag: Berlin, Heidelberg, New York, 1982; pp 234−276.

(34) Wasielewski, M. R.; Norris, J. R.; Crespi, H. L.; Harper, J. *J. Am. Chem. Soc.* **1981**, *103*, 7664−7665.

(35) Wasielewski, M. R.; Norris, J. R.; Shipman, L. L.; Lin, C.-P.; Svec, W. A. *Proc. Natl. Acad. Sci. U.S.A.* **1981**, *78*, 2957−2961.

(36) O'Malley, P. J.; Babock, G. T. *Proc. Natl. Acad. Sci. U.S.A.* **1984**, *81*, 1098−1101.

(37) Davis, M. S.; Forman, A.; Fajer, J. *Proc. Natl. Acad. Sci. U.S.A.* **1979**, *76*, 4170−4174.

(38) Käss, H.; Lubitz, W.; Hartwig, G.; Scheer, H.; Noy, D.; Scherz, A. *Spectrochimica Acta* **1998**, Part A *54*, 1141−1156.

(39) Lendzian, F. PhD Thesis, Freie Universität Berlin, Berlin, Germany, 1982.

(40) Astashkin, A. V.; Dikanov, S. A.; Tsvetskov, Y. D.; Goldfeld, M. G. *Chem. Phys. Lett.* **1987**, *134*, 438−443.

(41) Mac, M.; Tang, X.-S.; Diner, B. A.; McCracken, J.; Babock, G. T. *Biochemistry* **1996**, *35*, 12388−13293.

(42) Käss, H.; Bittersmann-Weidlich, E.; Andréasson, L.-E.; Bönigk, B.; Lubitz, W. *Chem. Phys. Lett.* **1995**, *194*, 419−432.

(43) Käss, H.; Lubitz, W. *Chem. Phys. Lett.* **1996**, *251*, 193−203.

(44) Käss, H.; Fromme, P.; Lubitz, W. *Chem. Phys. Lett.* **1996**, *257*, 197−206.

(45) Mac, M.; Bowlby, N. R.; Babcock, G. T.; McCracken, J. *J. Am. Chem. Soc.* **1998**, *120*, 13215−13223.

(46) Webber, A. N.; Su, H.; Bingham, S. E.; Käss, H.; Krabben, L.; Kuhn, M.; Schlodder, E.; Lubitz, W. *Biochemistry* **1996**, *35*, 12857−12863.

(47) Redding, K.; MacMillan, F.; Leibl, W.; Brettl, K.; Hahnley, J.; Rutherford, A. W.; Breton, J.; Rochaix, J.-D. *EMBO J.* **1998**, *17*, 50−60.

(48) Krabben, L.; Schlodder, E.; Jordan, R.; Carbonera, D.; Giacometti, G.; Lee, H.; Webber, A. N.; Lubitz, W. *Biochemistry* **2000**, *39*, 13012−13025.

(49) Moënne-Loccoz, P.; Robert, B.; Lutz, M. *Biochemistry* **1990**, *29*, 4740−4746.

(50) Nabedryk, E.; Leonhard, M.; Mäntele, W.; Breton, J. *Biochemistry* **1990**, *29*, 3242−3247.

(51) Breton, J.; Nabedryk, E.; Leibl, W. *Biochemistry* **1999**, *38*, 11585−11592.

(52) Nabedryk, E.; Leibl, W.; Breton, J. *Photosynth. Res.* **1996**, *48*, 301−308.

(53) Krauss, N.; Hinrichs, W.; Witt, I.; Fromme, P.; Pritzkow, W.; Dauter, Z.; Betzel, C.; Wilson, K. S.; Witt, H. T.; Saenger, W. *Nature* **1993**, *361*, 326−331.

(54) Jordan, P.; Fromme, P.; Klukas, O.; Witt, H. T.; Saenger, W.; Krauss, N., submitted for publication.

(55) Käss, H.; Rautter, J.;, Zweygart, W.; Struck, A.; Scheer, H.; Lubitz, W. *J. Phys. Chem.* **1994**, *98*, 354−363.

(56) Zweygart, W.; Thanner, R.; Lubitz, W. *J. Magn. Reson.* **1994**, *A109*, 172−176.

(57) Tränkle, E.; Lendzian, F. *J. Magn. Reson.* **1989**, *84*, 537−547.

(58) Atherton, N. M. *Principles of Electron Spin Resonance*; Ellis Horwood PTR Prentice Hall: New York, 1993.

(59) Norris, J. R.; Uphaus, R. A.; Crespi, H. L.; Katz, J. *J. Proc. Natl. Acad. Sci. U.S.A.* **1971**, *68*, 625−628.

(60) Miller, A.-F.; Brudvig, G. W. *Biochim. Biophys. Acta* **1991**, *1056*, 1−18.

(61) Prisner, T. F.; McDermott, A. E.; Un, S.; Norris, J. R.; Thurnauer, M. C.; Griffin, R. G. *Proc. Natl. Acad. Sci. U.S.A.* **1993**, *90*, 9485−9488.

(62) Bratt, P. J.; Rohrer, M.; Krzystek, J.; Evans, M. C. W.; Brunel, L.-C.; Angerhofer, A. *J. Phys. Chem. B* **1997**, *101*, 9686−9689.

(63) Zech, S.; Hofbauer, W.; Kamlowski, A.; Fromme, P.; Stehlik, D.; Lubitz, W.; Bittl, R. *J. Phys. Chem. B* **2000**, *104*, 9728−9739.

(64) Klette, R.; Törring, J. T.; Plato, M.; Möbius, K.; Bönigk, B.; Lubitz, W. *J. Phys. Chem.* **1993**, *97*, 2015−2020.

(65) Rigby, S. E. J.; Nugent, J. H. A.; O'Malley, P. J. *Biochemistry* **1994**, *33*, 10043−10050.

(66) Müh, F.; Rautter, J.; Lubitz, W. *Biochemistry* **1997**, *36*, 4155−4162.

(67) Lendzian, F.; Lubitz, W.; Scheer, H.; Bubenzer, C.; Möbius, K. *J. Am. Chem. Soc.* **1981**, *103*, 4635−4637.

(68) The rotational correlation time τ_R has been estimated from the Einstein−Debye relation $\tau_R = V_{eff} \cdot \eta / kT$, in which V_{eff} is the effective volume of the trimeric PS I complex ($\sim 2 \times 10^{-18}$ cm^3), η is the dynamic viscosity

of water ($\eta = 0.013$ P at $T = 283$ K), and k is the Boltzmann constant (for details see ref 39, cf. also ref 69).

(69) Chasteen, N. D.; Francavilla, J. *J. Phys. Chem*. **1976**, *80*, 867−871.

(70) Feher, G.; Hoff, A. J.; Isaacson, R. A.; Ackerson, L. C. *Ann. N.Y. Acad. Sci*. **1975**, *244*, 239−259.

(71) Hyde, J. S.; Rist, G. H.; Eriksson, L. E. G. *J. Phys. Chem*. **1968**, *72*, 4269−4276.

(72) Kurreck, H.; Bock, M.; Bretz, N.; Elsner, M.; Kraus, H.; Lubitz, W.; Müller, F.; Geisler, J.; Kroneck, P. M. H. *J. Am. Chem. Soc*. **1984**, *106*, 737−746.

(73) Bryant, D. A. In *The Photosystems: Structure, Function and Molecular Biology*; Barber, J., Ed.; Elsevier Science Publishers B. V.: Amsterdam, 1992; pp 501−549.

(74) Scheer, H.; Katz, J. J.; Norris, J. R. *J. Am. Chem. Soc.* **1977**, *99*, 1372−1381.

(75) Huber, M.; Lendzian, F.; Lubitz, W.; Tränkle, E.; Möbius, K.; Wasielewski, M. R. *Chem. Phys. Lett*. **1986**, *132*, 467−473.

(76) Plato, M.; Möbius, K.; Lubitz, W. In *Chlorophylls*; Scheer, H., Ed.; CRC Press: Boca Raton, FL, 1991; pp 1015−1046.

(77) Plato, M.; Lendzian, F.; Lubitz, W.; Möbius, K. In *The Photosynthetic Bacterial Reaction Center II: Structure, Spectroscopy and Dynamics*; Breton, J., Vermeglio, A., Eds.; Plenum Press: New York, 1992; pp 109−118.

(78) Chow, H.-C.; Serlin, R.; Strouse, C. E. *J. Am. Chem. Soc*. **1975**, *97*, 7230−7237.

(79) Lubitz, W.; Lendzian, F.; Plato, M.; Scheer, H.; Möbius, K. *Appl. Magn. Res.* **1997**, *13*, 531−551.

(80) If this assignment is to be correct, the spin density ratio between the two halves of $P_{700}^{+\bullet}$ would have to be 75:25 to 80:20. From a comparison of the assigned large CH_3 hfcs of $P_{700}^{+\bullet}$ and Chl $a^{+\bullet}$ in organic solvents (Tables 2 and 3), a somewhat larger asymmetry (∼85:15) between the dimer halves is deduced (see text).

(81) Käss, H. PhD Thesis, Technische Universität Berlin, Berlin, Germany, 1995.

(82) Carrington, A.; McLachlan, A. D. *Introduction to Magnetic Resonance with Applications to Chemistry and Chemical Physics*; Harper & Row: New York, 1969; p 137f.

(83) Rautter, J.; Lendzian, F.; Fetsch, A.; Schulz, C.; Kuhn, M.; Lin, X.; Williams, C. J.; Allen, J. P.; Lubitz, W. *Biochemistry* **1995**, *34*, 8130−8143.

(84) Sétif, P. In *The Photosystems: Structure, Function and Molecular Biology*; Barber, J., Ed.; Elsevier Science Publishers: Amsterdam, 1992; pp 471−499.

(85) den Blanken, H. J.; Hoff, A. J. *Biochim. Biophys. Acta* **1983**, *724*, 52−61.

(86) Knapp, E. W.; Fischer, S. F.; Zinth, W.; Sander, M.; Kaiser, W.; Deisenhofer, J.; Michel, H. *Proc. Natl. Acad. Sci. U.S.A.* **1985**, *82*, 8463−8467.

(87) Reddy, N. R. S.; Kolaczkowski, S. V.; Small, G. J. *J. Phys. Chem.* **1993**, *97*, 6934−6940.

(88) Plato, M.; Lubitz, W.; Lendzian, F.; Möbius, K. *Isr. J. Chem*. **1988**, *28*, 109−119.

(89) Sieckmann, I.; Brettel, K.; Bock, C.; van der Est, A.; Stehlik, D. *Biochemistry* **1993**, *32*, 4842−4847.

(90) Assuming a C_2 symmetric arrangement of two Chl *a* molecules and neglecting the possibility of charge-transfer contributions to $^3P_{700}$, it was concluded that the magnetic y (or x) axes of the triplet include an angle of 55° (±5°).[89] The methyl bond at position 12 and the molecular y axis of a Chl a molecule include an angle of 34°, according to the X-ray structure analysis.[78] From the ENDOR results performed on the single cystals, the angle between this methyl bond and the C_2 pseudosymmetry axis is 33°. If the Chl *a* molecules are arranged symmetrically to the C_2 axis, a calculation yields an angle of $2(33° + 34° - 90°) = 46°$ between the molecular y axes of the two halves. Taking the accuracy of ±5° into account, the result derived from the single-crystal ENDOR spectra is consistent with the interpretation of the EPR experiments on $^3P_{700}$.

(91) To exclude misinterpretations because of an erroneous definition of the orientation of the approximate C_2 axis in the RC's, we can consider alternatively the angle between the two C−CH_3 bonds at position 12 of the respective BChl molecules forming the primary donor. It has values of $2 \times 40.8°$ and $2 \times 37.8°$ in the *Rb. sphaeroides* structures[92,93] and $2 \times 38.5°$ in Rps. viridis.[94] If we assume that the pyrrol rings A of the respective BChl molecules are regular pentagons and, in a symmetric dimer, overlap in a perfect way the C−CH_3 bonds at positions 12 and the C_2 axes include angles of 36°.

(92) Ermler, U.; Fritzsch, G.; Buchanan, S. K.; Michel, H. *Structure* **1994**, *2*, 925−936.

(93) Chirino, A. J.; Lous, E. F.; Huber, M.; Allen, J. P.; Schenck, C. C.; Paddock, M. L.; Feher, G.; Rees, D. C. *Biochemistry* **1994**, *33*, 4584−4593.

(94) Ermler, U.; Michel, H.; Schiffer, M. *J. Bioenerg. Biomembr*. **1994**, *26*, 5−15.

(95) Schubert, W. D.; Klukas, O.; Saenger, W.; Witt, H. T.; Fromme, P.; Krauss, N. *J. Mol. Biol*. **1998**, *280*, 297−314.

(96) Rhee, K.-H.; Morris, E. P.; Barber, J.; Kühlbrandt, W. *Nature* **1998**, *396*, 283−286.

(97) Zouni, A.; Witt, H. T.; Kern, J.; Fromme, P.; Krauss, N.; Saenger, W.; Orth, P. *Nature* **2001**, in press.

(98) Telfer, A.; Lendzian, F.; Schlodder, E.; Barber, J.; Lubitz, W. In *Photosynthesis: Mechanisms and Effects*; Garab, G., Ed.; Kluwer Academic Publishers: Dordrecht, The Netherlands, 1998; Vol. II; pp 1061−1064.